

Ms. Ref. No.:	os-2016-70
Title:	Synoptic fluctuation of the Taiwan Warm Current in winter on the East China Sea shelf
Journal:	Ocean Science

Dear Dr. John M. Huthnance,

Thanks very much for your comments and assistances in editing our joint manuscript. We have made all the related corrections on the manuscript according to your comments.

Appended to this letter is the “Response to the referee” and a “marked-up manuscript”. The “Response to the referee” contains our point-by-point responses to the comments raised by you. The “marked-up manuscript” tracks our changes.

Once again, thank you very much for your kind support which significantly improved our manuscript. On behalf of all authors, we would like to express our great appreciation to you and the reviewers by mentioning all of you in the Acknowledgements.

Yours sincerely,

Jiliang Xuan, Daji Huang, Thomas Pohlmann, Jian Su, Bernhard Mayer, Ruibin Ding,
Feng Zhou
January 1, 2017

Response to the referee

Firstly a question. You are discussing winter but refer to the south-west “monsoon”. Is “monsoon” the correct word in winter as well as summer, or should it be “wind”? [North-east monsoon is winter is OK, I think].

Author’s response: We agree that the statement of “southwesterly monsoon in winter” is wrong in the manuscript. Revisions have been made in two aspects:

- 1) The word “monsoon” was changed to “wind” when discussing the southwesterly wind in winter.
- 2) The statements relating to wind direction and current direction throughout the manuscript were modified to be more accurately according to their actual directions, e.g., “northerly monsoon” was changed to “northeasterly monsoon”, “northward TWC” was changed to “northeastward TWC” etc.

Author’s changes in manuscript: We have revised the above mentioned “words” and “phrases” throughout the manuscript.

(Abstract)

Line 34. Omit “, extending in the region”

Author’s response: Agree.

Author’s changes in manuscript: Line 33: Omit “, extending in the region”.

Lines 34-35. “fluctuations . . alongshore . . are important for . . cross-shore transports.” This reads strangely.

Author’s response: We have now revised the statement.

Author’s changes in manuscript: Line 34-35: “The fluctuations are generally strong in the alongshore direction, in particular at the latitudes 26.5 °N and 28 °N where they are important for the local cross-shore transports” **was changed to** “The fluctuations are generally strong both in the alongshore and cross-shore directions, in particular at the latitudes 26.5 °N and 28 °N”.

(1. Introduction)

Line 51. Better “. . its weak mean surface velocity . .”

Author’s response: Agree.

Author’s changes in manuscript: Line 51: “its surface weak mean velocity” was changed to “its weak mean surface velocity”.

Lines 60-61. Better “. . fluctuations still lack study; the fluctuations . . may be complicated”

Author’s response: Agree.

Author’s changes in manuscript: Line 61-62: “fluctuations are still lack of study, regarding that the fluctuations on the whole shelf of the ECS may be more complicated due to the complex bottom topography” **was changed to** “fluctuations

still lack study; the fluctuations on the whole shelf of the ECS may be complicated due to the complex bottom topography”.

Line 67. Intermittency does not have an amplitude: “. . the variations of the TWC . . have an amplitude . .”

Author’s response: Thanks.

Author’s changes in manuscript: Line 67: “intermittency” was changed to “variations”, and “has” was changed to “have”.

Line 68. You might want to change this to: “. . the variations of the TWC . . cause a . .”

Author’s response: Agree.

Author’s changes in manuscript: Line 68: “intermittency” was changed to “variations”, and “causes” was changed to “cause”.

Line 86. “mainly occur close to those specific isobaths. . .”

Author’s response: Agree.

Author’s changes in manuscript: Line 86: “mainly occur in those specific isobaths” was changed to “mainly occur close to those specific isobaths”.

Lines 93-94. “. . indicating a strong synoptic fluctuation . .” [“stronger” implies a comparison which you do not make]

Author’s response: Thanks.

Author’s changes in manuscript: Line 93-94: “much stronger” was changed to “strong”.

Lines 124-125. Better “. . investigate wintertime TWC synoptic fluctuations and their mechanisms. The rest . .”

Author’s response: Agree.

Author’s changes in manuscript: Line 125: “synoptic fluctuations and their mechanisms of the wintertime TWC” was changed to “wintertime TWC synoptic fluctuations and their mechanisms”.

(2.1)

Line 160. “. . velocity set to zero. . .”

Author’s response: Agree.

Author’s changes in manuscript: Line 160: “setted” was changed to “set”.

Line 161. “. . and at the lateral boundaries a sponge layer”

Author’s response: Agree.

Author’s changes in manuscript: Line 161: “and that at the lateral boundaries sponge layer was used” was changed to “and at the lateral boundaries a sponge layer was used”.

Line 163. Delete “of”

Author’s response: Agree.

Author’s changes in manuscript: Line 163: “of” was deleted.

(2.2)

Line 204. “direction as from . .”

Author’s response: Agree.

Author’s changes in manuscript: Line 204: “directing” was to changed “direction as”.

Lines 205-206. “. . cross-shore direction is from northwest . .(128 °), normal to the isobaths. The alongshore . .”

Author’s response: Agree.

Author’s changes in manuscript: Line 205-206: “The positive cross-shore direction is the mean normal direction of the isobaths from northwest (308 °) to southeast (128 °)” **was changed to** “The positive cross-shore direction is from northwest (308 °) to southeast (128 °), normal to the isbaths”.

Lines 229-230. “. . i.e. that the mean alongshore component . . than the mean cross-shore component, the magnitude . .” Maybe the last part of this sentence “the magnitude . . alongshore fluctuations” should move to the beginning of the sentence.

Author’s response: We have now revised the statement.

Author’s changes in manuscript: Line 228-232: “In contrast to the anisotropic feature for the mean currents (Fig. 3), i.e., that the alongshore component is nearly one order of magnitude larger than the cross-shore component in the mean condition, the magnitude of the cross-shore fluctuations is comparable to the alongshore fluctuations” **was changed to** “The magnitude of the cross-shore fluctuations is comparable to the alongshore fluctuations. This is different to the anisotropic characteristic of the mean currents (Fig. 3), for which the alongshore component is nearly one order of magnitude larger than the cross-shore component”.

(2.4)

Line 269. “comparably” -> “comparatively”

Author’s response: Agree.

Author’s changes in manuscript: Line 270: “comparably” was changed to “comparatively”.

Equation (5) and line 273. Velocity at the bottom might better be vector “V_b”.

Author’s response: Agree.

Author’s changes in manuscript: Line 271-274: “U_b” was changed to “V_b”.

(3.1).

Line 285. Can omit “a horizontal structure with”

Author's response: Agree.

Author's changes in manuscript: Line 285: “a horizontal structure with” was deleted.

Line 297. Delete final “a”

Author's response: Agree.

Author's changes in manuscript: Line 298: “a different cooling occurs” was changed to “different cooling occurs”.

Lines 298 to 301. I am confused by the directions here. If “offshore” (line 299) is to the south-east then the vertical shear would be northeastward (not as stated on line 299), which does result in a southwestward flow component increasing downwards. Whether this weakens the northeastward TWC depends on assumptions about where in depth the flow is unchanged. This also needs better explanation to justify “effects of baroclinicity” in line 303.

Author's response: Agree with your argument. A northeastward thermal current (vertical shear of current) is generated by a northwestward density gradient, which results in a northeastward flow (TWC) increasing upwards.

The subsurface current core is caused by the combined effects of wind friction (which results in a southwestward flow increasing downward) and baroclinicity (which results in a northeastward flow increasing upward).

Author's changes in manuscript:

Line 292-308: The whole paragraph was rewritten as follows. “We further examined the subsurface current core using the depth of the VMV (Fig. 5b). We found that the VMV of the TWC was located 40–60 m below the surface at the inshore branch and 20–40 m below the surface at the offshore branch. Figure 6 shows the VMV positions in the subsurface layer; it also illustrates that the depth of the subsurface VMV in the inshore branch was deeper than that in the offshore branch. The difference can be explained by the combined effects of baroclinicity and wind friction. Assuming a relatively spatially homogeneous heat loss, different cooling occurs, due to the smaller heat capacity of the shallow coastal water compared to the deeper offshore waters; hence generating a northwestward horizontal density gradient leading to a northeastward thermal current (vertical current shear) according to the thermal wind relationship, resulting in an increasing of northeastward flow increasing upward. The northeasterly wind in winter weakens the northeastward TWC, particularly in the upper layer, which leads to the formation of the subsurface VMV. Therefore, the fact that the depth of the subsurface current core in the inshore branch is greater than that in the offshore branch indicates that a weaker baroclinicity or a stronger wind friction on the inshore branch than on the offshore branch.”

Line 304. “. . than on the . .”

Author's response: Agree.

Author's changes in manuscript: Line 308: “than the offshore branch” was changed to “than on the offshore branch”.

(3.2)

Lines 334-335. “. . had a strong cross-shore component which means . .”

Author’s response: Agree.

Author’s changes in manuscript: Line 339: “had a strong magnitude in the cross-shore direction” was changed to “had a strong cross-shore component”.

Lines 337-338. This implies that the ZMCC might be very wide, out to as much as 100m depth. This is a surprise to the reader because 30-100m depth was supposed to be the region for the TWC inshore branch.

Line 339. “episodically” means the TWC inshore branch is sometimes present and sometimes absent. For this, the fluctuations need to be more than “significant”; they sometimes need to be larger than the mean.

Author’s response: We agree that the statements of “ZMCC and TWC meet between the 30 and 100 m isobaths” and “episodic occurrence of TWC inshore branch” at the first sight are contradictory. However, one has to clearly distinguish between the mean flow and the variability here. Our statement that the dominant region of the TWC inshore branch is located between the 30 and 100 m isobaths, was based on the wintertime climatological density distribution, and additionally, by our simulations of the climatological mean currents (Figs. 5 and 6). However, when considering the variability of the current system, it can be observed that strong fluctuations occur, leading to the situation that the TWC becomes episodically and the ZMCC might be very wide for certain periods, as observed at the site off the Zhe-Min coast (Fig. 4). To clarify these points, we revised the following statement.

Author’s changes in manuscript: Line 341-348: “In the inshore area, the fluctuation was located in a wide region between the 30 and 100 m isobaths, where the southwestward flowing ZMCC and the northeastward directed TWC meet. As deduced from the standard deviation, the currents fluctuated significantly in the alongshore direction, indicating that the TWC inshore branch occurred episodically.” **was changed to** “In the inshore area, the fluctuations were influencing a wide region between the 30 and 100 m isobaths, with a magnitude sometimes being larger than the mean flow (Fig. 5a). These strong fluctuations led to an episodic occurrence of the TWC inshore branch, as observed at the site off the Zhe-Min coast (Fig. 4, high temperature). When the TWC inshore branch was weakened due to these fluctuations, the ZMCC might even dominate a wide region outside of the 100 m isobath, especially at the surface (Fig. 4, low temperature.)”.

Lines 347-348. Better “. . Richardson et al., 2013), i.e. where the Richardson number equals the critical value 0.25 in this paper . .”

Author’s response: Agree.

Author’s changes in manuscript: Line 357: Changed to “. . Richardson et al., 2013), i.e. where the Richardson number equals the critical value 0.25 in this paper . .”.

Line 353. Omit “Hence”. [Correlation does not show what causes what. The rest

of the sentence is OK because wind and cooling are forcings.]

Author's response: Thanks.

Author's changes in manuscript: Line 362: "Hence" was deleted.

Line 359. "account for 54% . . (Fig. 9), associated . . ." ["which" can only refer to the object immediately before].

Author's response: Thanks.

Author's changes in manuscript: Line 368: Changed to "account for 54% . . (Fig. 9), associated . .".

Line 365. Omit "great".

Author's response: Agree.

Author's changes in manuscript: Line 374: Omitted "great".

Lines 369-372. There is some repetition here.

Author's response: We have now revised the statement.

Author's changes in manuscript: Line 378-382: "The spatial pattern of the second EOF mode (EOF2, Fig. 9b) shows a synoptic fluctuation in the inshore area. The fluctuation mainly varied in the alongshore direction, which indicates the episodic occurrence of the TWC inshore branch. The area with alongshore fluctuation (Fig. 9d) larger than 0.1 m/s was located between the 30 and 100 m isobaths, which demonstrates that the TWC could also episodically affect this area" **was changed to** "The spatial pattern of the second EOF mode (EOF2, Fig. 9b) shows a synoptic fluctuation in the inshore area. The area with alongshore fluctuation (Fig. 9d) larger than 0.1 m/s was located between the 30 and 100 m isobaths, which demonstrates that the TWC could episodically affect this area".

Line 374. "great" -> "larger".

Author's response: Agree.

Author's changes in manuscript: Line 383: "great" was changed to "larger".

Line 390. "would then replace the . ."

Author's response: Agree.

Author's changes in manuscript: Line 399: "which replaces" was changed to "which would then replace".

Line 391. "Feb. 14-18"? This sentence is not very convincing. What about the deepening on 7-10 February?

Author's response: Yes, you are right. Probably due to the fact that the wind shown in Fig. 11 is regionally averaged, while the mixed layer depth given in Fig. 8 represents conditions at a specified location, there is not such a clear connection between these two parameters. Therefore, we deleted this unconvincing statement.

Author's changes in manuscript: Line 399-401: deleted "Together with the effect of net surface heat flux, the stronger northerly monsoon during Jan. 5-13, Jan. 19-25 and

Feb. 16-18 causes the deepening of the mixed layer (P2, Fig. 8).”

(4 Discussion)

Line 443. Omit first “The”. “winters” – please state here if this is December – March or January – February.

Author’s response: We have now revised the statement.

Author’s changes in manuscript: Line 452: “The simulated results in the winters” was changed to “Simulated results in the winters (December-March)”.

Line 446. “. . were present in all winters from 2009 to 2013.”

Author’s response: Agree.

Author’s changes in manuscript: Line 455-456: Changed to “. . were present in all winters from 2009 to 2013”.

Line 452. “. . manifested by two . .” [delete “with”]

Author’s response: Agree.

Author’s changes in manuscript: Line 461: deleted “with”.

(4.2)

Line 538. Do you mean “exchange” or just that water between the 30 and 100m isobaths may be either ZMCC or TWC water.

Author’s response: Thanks. It should read: “water between the 30 and 100m isobaths may be either ZMCC or TWC water”.

Author’s changes in manuscript: Line 546-548: “water exchange between the ZMCC water and the TWC water exists in the area between the 30 and 100 m isobaths” was changed to “water between the 30 and 100 m isobaths may be either ZMCC or TWC water”.

Lines 543-544. “. . considered, not short-term . .” [Omit “in the relation . . and no”]

Author’s response: Agree.

Author’s changes in manuscript: Line 552-553: “only wind-induced synoptic fluctuations are considered in the relations to the episodic events and no short-term extreme storm events” was changed to “only wind-induced synoptic fluctuations are considered, not short-term extreme storm events”.

Lines 558-559. “(Fig. 5a). Thus the offshore transports . .”

Author’s response: Agree.

Author’s changes in manuscript: Line 569: “This also indicates that” was changed to “Thus”.

(5 Conclusions)

Line 584. “. . was nearly balanced . .”

Author's response: Agree.

Author's changes in manuscript: Line 594: “was balanced” was changed to “was nearly balanced”.

Figures; generally it is better have units named on color scales.

Author's response: Thanks. We have now added units on all the color scales.

Author's changes in manuscript: added color scales in Figure 1 (line 894), Figure 5 (line 922), Figure 8 (line 944) and Figure 12 (line 969).

Figure 1 caption (lines 779, 875) “derived from the GDEM . . .”

Author's response: Agree

Author's changes in manuscript: Line 792, 895: “derived the GDEM” was changed to “derived from the GDEM”.

Figure 2 caption (lines 788, 884) “lines (right) show . . .”

Author's response: Agree.

Author's changes in manuscript: Line 801, 905: “lines show” was changed to “lines (right) show”.

Figure 5 caption (lines 807, 906) “ECS, shown by color. Sections . . .”

Author's response: Agree.

Author's changes in manuscript: Line 820, 927: “in the ECS” was changed to “in the ECS, shown by color”.

Figure 7 caption. Explain black arrows. Lines 818, 919: “. . . the branches' representative . . .”

Author's response: Thanks. We have now added an annotation for the black arrows.

Author's changes in manuscript: Line 830, 939: “Current standard deviation” was changed to “Current standard deviation (black arrows)”. Line 833, 942: “their representative points” was changed to “the branches' representative points”.

Figure 8 caption (lines 821, 923) “. . . currents (m/s, shown by color scale) for . . .”

Author's response: Agree.

Author's changes in manuscript: Line 835, 945: Changed to “currents (m/s, shown by color scale)”.

Figure 9 caption (lines 827, 930) “. . . (f) EOF2 cross-shore component (all shown by color scale). The 30,” Explain black arrows.

Author's response: We have revised the caption and added an annotation for the black arrows.

Author's changes in manuscript: Line 842-843, 953-954: “(f) EOF2 cross-shore component” was changed to “(f) EOF2 cross-shore component (all shown by black arrows with the color representing the magnitude)”.

Figure 10 caption (lines 831, 935) “along” -> “across” or “at” (twice).

Author’s response: Agree.

Author’s changes in manuscript: Line 847, 853, 959, 966: “along” was changed to “across”.

Figure 12 caption (lines 841, 947) “. . Eq. (5) (shown by the color scale; units: . .”

Author’s response: Agree.

Author’s changes in manuscript: Line 857-858, 971-972: “(units: $10^{-4} \text{ m}^2/\text{s}^2$)” was changed to “(shown by black arrows with the color representing the magnitude; units: $10^{-4} \text{ m}^2/\text{s}^2$)”.

Figure 14 caption (lines 850, 959). What do the black arrows represent on the EOF plots?

Author’s response: We have revised the caption and added an explanation for the black arrows.

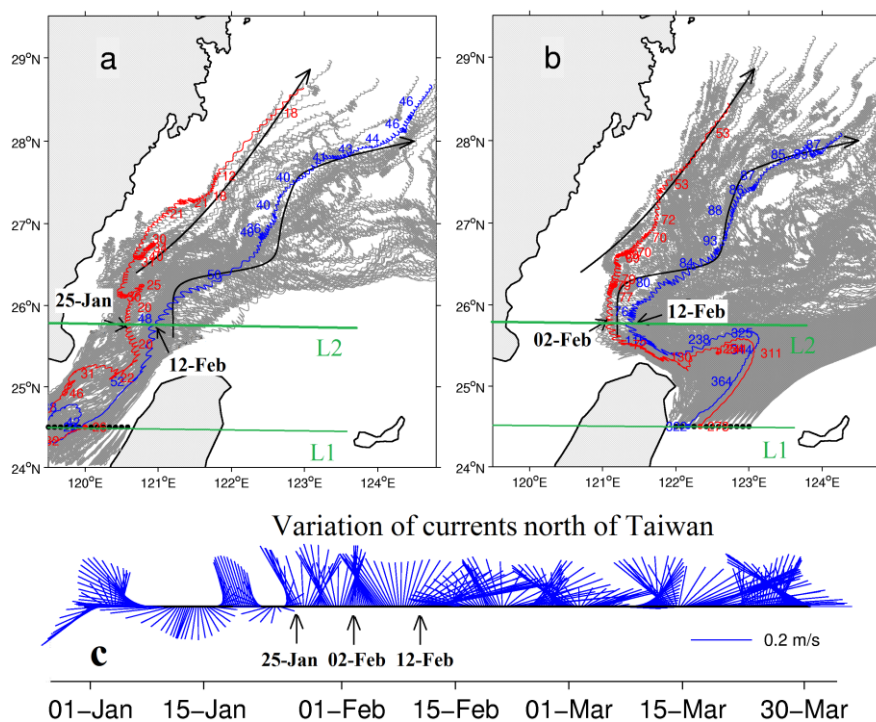
Author’s changes in manuscript: Line 867-871, 984-988: Changed to “The black arrows in the upper panels show the velocity (m/s) in the layer of VMV with the color representing the current speed. The two blue arrows with label IB and OB represent the flow axes of the inshore branch and offshore branch, respectively. The black arrows in the middle panels and bottom panels represent the EOF components (m/s) with their magnitude represented by color scales”.

Figure 15 caption (lines 858, 968). This is confusing. If P1 varies in time it could be anywhere and therefore useless.

Author’s response: We have now revised Figure 15 and its caption.

Author’s changes in manuscript:

Line 990: added two lines (L1 and L2) in Figure 15.



Line 874-876, 992-994: added the statement that “The green lines L1 and L2 indicate the starting latitude of the tracers (24.5 °N) and the latitude which is representative for synoptic fluctuations north of Taiwan (25.8 °N), respectively”.

Line 876, 994: Changed the statement to “The black dots represent the release locations of tracers originated from line L1”.

Line 879-880, 997-998: Changed the statement to “The dates show the times when selected tracers cross the latitude indicated by line L2”.

.

1 **Synoptic fluctuation of the Taiwan Warm Current in winter on the East China Sea shelf**

2 Jiliang Xuan¹, Daji Huang^{1, 2}, Thomas Pohlmann³, Jian Su³, Bernhard Mayer³, Ruibin Ding^{2,1}, Feng Zhou^{1, 2}

3

4 ¹State Key Laboratory of Satellite Ocean Environment Dynamics, Second Institute of Oceanography,

5 State Oceanic Administration, Hangzhou, China

6 ²Ocean College, Zhejiang University, Zhoushan, China

7 ³Institute of Oceanography, University of Hamburg, Hamburg, Germany

8 *Correspondence to:* Daji Huang (djhuang@sio.org.cn)

9 **Highlights**

- 10 ● Synoptic fluctuations of the wintertime Taiwan Warm Current appear mainly in two areas: north of
11 Taiwan and the inshore area
- 12 ● Synoptic fluctuation is mainly driven by the Taiwan Strait Current north of Taiwan and by wind in
13 the inshore area
- 14 ● Large Taiwan Strait Current intrusion generates a cross-shore transport from the coastal area to the
15 offshore area
- 16 ● Winter monsoon affects the alongshore transport of Taiwan Warm Current water between the 30
17 and 100 m isobaths
- 18 ● Winter monsoon affects the cross-shore transport of Taiwan Warm Current water at the latitudes
19 26.5 °N and 28 °N

20

21 **Abstract.** The seasonal mean and synoptic fluctuation of the wintertime Taiwan Warm Current (TWC)
22 were investigated using a well validated finite volume community ocean model. The spatial distribution
23 and dynamics of the synoptic fluctuation were highlighted. The seasonal mean of the wintertime TWC
24 has two branches: an inshore branch between the 30 and 100 m isobaths and an offshore branch between
25 the 100 and 200 m isobaths. The Coriolis term is much larger than the inertia term and is almost balanced
26 by the pressure gradient term in both branches, indicating the geostrophic balance of the mean current.
27 Two areas with significant fluctuations of the TWC were identified during wintertime. One of the areas
28 is located to the north of Taiwan with velocities varying in the cross-shore direction. These significant
29 cross-shore fluctuations are driven by barotropic pressure gradients associated with the intrusion of the
30 Taiwan Strait Current (TSC). When a strong TSC intrudes to north of Taiwan, the isobaric slope tilts
31 downward from south to north, leading to a cross-shore current from the coastal area to the offshore area.
32 When the TSC intrusion is weak, the cross-shore current to the north of Taiwan is directed from offshore
33 to inshore. The other area of significant fluctuation is located in the inshore area, ~~extending in the region~~
34 between the 30 and 100 m isobaths. The fluctuations are generally strong both in the alongshore and
35 cross-shore directions, in particular at the latitudes 26.5°N and 28°N ~~where they are important for the~~
36 ~~local cross-shore transports~~. Wind affects the synoptic fluctuation through episodic events. When the
37 northeasterly monsoon prevails, the ~~south~~southwestward Zhe-Min Coastal Current dominates the inshore
38 area associated with a deepening of the mixed layer. When the winter monsoon is weakened or the
39 southwesterly wind prevails, the northeastward TWC dominates in the inshore area.

40

41 **Keywords:**

42 Synoptic fluctuation, East China Sea, Taiwan Warm Current, Taiwan Strait Current, Kuroshio

43

44 1 Introduction

45

46 On the East China Sea (ECS) shelf, the mean path of the Taiwan Warm Current (TWC) has two branches:
47 the inshore branch along the 50 m isobath and the offshore branch along the 100 m isobath (Su and Pan,
48 1987). The summer TWC has been well studied because the current is stationary and strong, with an
49 average speed of 0.3 m/s (Guan, 1978; Fang et al., 1991; Isobe, 2008; Yang et al., 2011, 2012). The
50 spatial structure and temporal variation of the wintertime (December to March) TWC are less known due
51 to its ~~surface~~-weak mean surface velocity, according to a climatological structure of the surface current
52 in the ECS mapped by Qiu and Imasato (1990).

53

54 The wintertime TWC on the ECS shelf shows synoptic fluctuations (Cui et al., 2004; Zhu et al., 2004;
55 Zeng et al., 2012; Huang et al., 2016). These synoptic fluctuations show some features common with
56 those over other continental shelves, i.e., they have periods between 3 and 15 days and are associated
57 with coastal sea level changes, which can be explained by local winds or by coastal trapped waves (Huyer,
58 1990; Brink, 1991; Huthnance et al., 1986). Huang et al. (2016) have shown that the wind was a main
59 physical factor which caused the temporal variation of the wintertime currents at the synoptic scale in
60 the coastal area of the ECS. However, the dominant physical factors of the TWC fluctuations ~~are~~ still
61 ~~lack-of~~ study; ~~regarding that~~ the fluctuations on the whole shelf of the ECS may be ~~more~~-complicated
62 due to the complex bottom topography, alternating ~~monsoon-wind~~ forcing and conjunction of several
63 current systems such as the Kuroshio Current, the Taiwan Strait Current (TSC) and the Zhe-Min Coastal
64 Current (ZMCC). These synoptic fluctuations are also known to influence the regional material transport,

65 especially when the amplitude of the fluctuations is comparable to, or even larger than, the mean current.
66 On the ECS shelf, some recent observations have shown that the TWC has an episodic wintertime feature
67 (Zhu et al., 2004) and the intermittency-variations of the TWC in winter haves an amplitude as large as
68 0.2 m/s (Zeng et al., 2012). Moreover, it has been observed that the intermittency-variations of the TWC
69 in winter causes a cross-shore current which is closely linked to the alongshore component (Huang et al.,
70 2016). Therefore, we focus on studying the spatial patterns of synoptic fluctuations to better understand
71 the role of the wintertime TWC on the cross-shore water exchange.

72

73 A comparison between the wintertime climatological density (Fig. 1a) and synoptic density distributions
74 observed during two surveys (Figs. 1b and 1c) suggests that two distinct areas with significant synoptic
75 fluctuations exist. The climatological density is taken from the Generalized Digital Environment Model
76 (GDEM, Carnes, 2009) data, and the two surveys were carried out in February 2007 by two research
77 vessels. Because the isopycnal lines are closely related to geostrophic currents, we can infer the strength
78 of the TWC from the horizontal gradient of the isopycnals between $24\text{-}\sigma_t$ and $25\text{-}\sigma_t$ contours (Fig. 1a).
79 This accounts for the fact that in winter the water mass of TWC is located in this density range [according
80 to the hydrography analysis of Su et al. (1994)]. The two-branch structure of the TWC can be inferred
81 from the wintertime climatological density. In this paper, we defined that the near-coast area is the area
82 between the coast and 30 m isobath where the ZMCC occurs; the inshore area is the area between the 30
83 and 100 m isobaths where the TWC inshore branch dominates; and the offshore area is the region between
84 the 100 and 200 m isobaths where the TWC offshore branch prevails. According to the hydrographic
85 data analysis and numerical interpretation by Su and Pan (1987), the TWC inshore and offshore branches
86 mainly occur close to those specific isobaths. However, these two branches were missing during the

87 two synoptic surveys (Figs. 1b and 1c), indicating strong synoptic fluctuations of the TWC on the ECS
88 shelf. Furthermore, the density anomalies between the two surveys and the GDEM data (Figs. 1d and 1e)
89 indicate that the most significant fluctuations are located north of Taiwan and in the inshore area. Both
90 surveys show negative density anomalies north of Taiwan, indicating that the TWC was weak and that
91 less low-density coastal water was transported to the ECS shelf during the observational periods. The
92 density anomalies in the inshore area show different patterns for the two synoptic surveys, with a positive
93 anomaly in the first survey (Fig. 1d) and a negative anomaly in the second (Fig. 1e), indicating a ~~much~~
94 ~~stronger~~ synoptic fluctuation in the inshore area.

95

96  Figure 1

97

98 Candidate factors for driving these synoptic fluctuations are local wind, surface cooling, and the upstream
99 currents of the Kuroshio Current and the TSC. As discussed by Huyer (1990), wind is often considered
100 as the major driving mechanism of synoptic fluctuations of the wintertime TWC. The northeasterly
101 monsoon wind in winter blows against the northeastward TWC and produces a southwestward ZMCC
102 (Chuang and Liang, 1994; Oey et al., 2010). Zhu et al. (2004) suggested that the occurrence and duration
103 of the TWC are associated with the meandering of the Kuroshio Current north of Taiwan. The
104 northeastward TSC, as an upstream flow of the TWC, also influences the synoptic fluctuation of the
105 wintertime TWC. Hong et al. (2011) and Hu et al. (2010) summarized that the temporal and spatial
106 variation of TSC is modulated by strong ~~monsoonwind~~ forcing, complex topography and circulation in
107 the northern South China Sea as well as coastal water input and the Kuroshio intrusion. Guan and Fang
108 (2006) showed evidence that the TSC and the TWC merge in the area between the Taiwan Strait and the

109 Zhe-Min coastal region. Takahashi and Morimoto (2013) pointed out that the temporal variation of the
110 TWC is characterized by the propagation of vorticity anomalies originating from northeast of the Taiwan
111 Strait, which further demonstrated that the fluctuations of TWC was associated with its upstream currents
112 such as the TSC.

113

114 To explore the spatial distribution of synoptic fluctuations of the wintertime TWC on the ECS shelf,
115 current data with high resolution in both space and time are required. Previous studies on the wintertime
116 TWC were based on cruise surveys (Su and Pan, 1987; Chen et al., 1994; Chen and Wang, 1999),
117 anchored mooring observations (Zhu et al., 2004; Zeng et al., 2012; Huang et al., 2016) and numerical
118 simulations (Guo et al., 2003, 2006; Yang et al., 2011, 2012; Xuan et al., 2012, 2016). The observation
119 data are limited in terms of temporal and spatial coverage; hence, they cannot fully reveal the synoptic
120 fluctuations of the TWC and their regional differences. Numerical simulations provide a promising
121 approach for studying the overall structure and driving mechanisms of synoptic fluctuations of the TWC
122 in more detail.

123

124 In this study, the Finite Volume Coastal Ocean Model (FVCOM; Chen et al., 2003) is used to investigate
125 wintertime synoptic fluctuations and their mechanisms ~~of the wintertime TWC~~. The rest of this paper is
126 organized as follows. In Sect. 2, we provide a description of methods and validation. The mean
127 distribution, synoptic fluctuations, and dynamic diagnostics of the wintertime TWC are given in Sect. 3.
128 The impact of synoptic fluctuation on water exchange is further discussed in Sect. 4, followed by
129 conclusions in Sect. 5.

130

131 **2 Methods and validation**

132 **2.1 Model configuration**

133 To investigate the currents (TWC, Kuroshio Current, ZMCC, etc.) and their synoptic fluctuations on the
134 ECS shelf, a 3-D unstructured-grid (Fig. 2, left panel) FVCOM is developed for the entire Bohai, Yellow,
135 and East China Seas (part of the Japan/East Sea, and part of the Pacific Ocean). A regional refinement of
136 the resolution (approximately 3 km) is specified around the ECS shelf break at the 200 m isobaths, where
137 a strong excursion of the Kuroshio Current also occurs. The General Bathymetric Chart of the Oceans
138 (GEBCO) provides high-resolution (approximately 1 km) bathymetric data (Smith and Sandwell, 1997).
139 Twenty vertical layers with 76954 triangle cells were specified in the water column in a sigma-stretched
140 coordinate system.

141

142 The driving forces of the numerical simulation include tides, river discharge, surface heat fluxes, wind,
143 and open boundary conditions. Harmonic constants of 11 major tidal constituents (M_2 , S_2 , N_2 , K_2 , K_1 , O_1 ,
144 P_1 , Q_1 , M_4 , MS_4 , and MN_4) were used; these are based on the Oregon State University global inverse
145 tidal model TPXO.7.0 (Egbert et al., 1994; Egbert and Erofeeva, 2002). The daily-mean river discharge
146 of the Changjiang and Huanghe were taken from publicly available observation data at the Datong
147 hydrometric station (<http://yu-zhu.vicp.net/>). Other rivers were not included because of their small
148 discharges, e.g., the Qiantang River, with the largest runoff from the Zhejiang coast, has a climatological
149 mean discharge in winter of about $230 \text{ m}^3/\text{s}$, which is nearly negligible compared to the Changjiang
150 winter discharge of about $11500 \text{ m}^3/\text{s}$. The daily-mean heat fluxes were from the objectively analyzed
151 air-sea fluxes (Yu and Weller, 2007), and the 3-hourly wind stress and 10 m wind speed data was from
152 the ERA-40 re-analysis (Uppala et al., 2005). The open boundary conditions, including daily temperature,

153 salinity, and fluxes at the Taiwan Strait, the western Pacific Ocean, and the Japan/East Sea, were obtained
154 from the Hybrid Coordinate Ocean Model (Bleck, 2002) and interpolated onto the FVCOM model grid
155 points. The temporal resolution of all the driving force fields is better than or equal to one day, which is
156 essential to resolve synoptic fluctuations.

157

158 The hindcast outputs of sea surface height, temperature, salinity, and velocities for the five years of
159 simulation from 2009 to 2013 are used, following three spin-up years (2006-2008) initiated with the
160 temperature and salinity taken from the Hybrid Coordinate Ocean Model and velocity ~~setted~~ to zero. The
161 initial conditions are ramped-up over a period of 30 days and ~~that~~ at the lateral boundaries a sponge layer
162 was used with the same method as Chen et al. (2008). The model time step was 15 seconds for the 2-D
163 barotropic mode ~~of~~ and 90 seconds for the 3-D baroclinic mode. All of the output fields were processed
164 with a tidal filter (Godin, 1972) to remove tidal oscillations (considering that the major time scale of
165 synoptic fluctuations in this study area is 3–15 days).

166

167 Since the currents in 2009 could partly be validated by means of available observational data (see Sect.
168 2.2), the currents from January 1 to February 28, 2009 were selected for analysis of the wintertime TWC.

169

170 **2.2 Validation of the mean currents and synoptic fluctuations**

171 The mean currents, e.g., the Kuroshio Current, the TWC, and the ZMCC, were calculated by averaging
172 the outputs of January and February 2009. We validated the mean currents in terms of circulation
173 structure, boundary fluxes, and coastal currents.

174

175 The FVCOM has reproduced almost all of the known circulation structure in the ECS in winter. The
176 surface mean currents (Fig. 2) shows three major currents: the Kuroshio Current, the TWC, and the
177 ZMCC. The Kuroshio Current, with a speed of about 1 m/s, enters the ECS just northeast of Taiwan and
178 flows along the shelf break up to the northern area and ultimately leaves the ECS through the Tokara
179 Strait. Both the route and strength of the Kuroshio are comparable with those reported in the literature
180 (Guan, 1978; Qiu and Imasato, 1990). The TWC has two northeastward branches, one inshore (between
181 the 30 and 100 m isobaths) and another offshore (between the 100 and 200 m isobaths), which is
182 consistent with Su and Pan (1987). The southsouthwestward directed ZMCC in the nearshore area from
183 the Changjiang Estuary to the Taiwan Strait agrees well with that reported in previous studies (Guan and
184 Mao, 1982; Zeng et al., 2012).

185

186 The simulated volume transports across the Taiwan Strait, the East Taiwan Channel, the Tsushima Strait,
187 the Tokara Strait, and the shelf break of the 200 m isobath were validated using results from the literature
188 (Table 1). The simulated transports were accurate enough to reproduce volume transport (1.22 Sv)
189 through the Taiwan Strait which is closer to the observation value (1.20 Sv) from Isobe (2008) than
190 former model results. The volume transports across the Taiwan Strait and the Tokara Strait, and the cross-
191 shore exchange, affected the path and magnitude of the TWC. The annual mean transport across the 200
192 m isobath toward the shelf is 1.66 Sv, which is balanced by the inflow from the Taiwan Strait (1.22 Sv)
193 and the outflow through the Tsushima Strait (2.85 Sv).

194

195

Figure 2

196

Table 1

198

199 Figure 3 shows a comparison between simulation and observation results for the alongshore currents and
200 the cross-shore currents on the ECS shelf. The observational data were obtained from four mooring
201 surveys (Fig. 2, red stations) off the Zhe-Min coast (Zeng et al., 2012). The observed and simulated
202 currents were both averaged for the observational period, which was from January 1 to February 28,
203 2009. Using the same method as in Huang et al. (2016), we defined the positive alongshore current
204 ~~directing direction as~~ from southwest (218°) to northeast (38°), which is the mean tangential direction of
205 the isobaths on the southwestern shelf of the ECS. The positive cross-shore direction is ~~the mean normal~~
206 ~~direction of the isobaths~~ from northwest (308°) to southeast (128°), normal to the isobaths. The alongshore
207 components (Figs. 3a and 3b) show that the ZMCC flows southwestward parallel to the coast in winter,
208 with a maximum speed of 0.15 m/s along the 30 m isobath. The TWC flows northeastward with a speed
209 of 0.05 m/s, and the core is located in the lower layer at about 50 m at Station 4. The cross-shore
210 component (Figs. 3c and 3d) is much weaker than the alongshore components, and it shows a complex
211 spatial pattern. It flows offshore in the upper layer and onshore in the lower layer at Station 1. Moreover,
212 it mainly flows onshore at Station 2, and it flows offshore in the entire water column at Stations 3 and 4.
213 Altogether, the simulated pattern and magnitude both of the alongshore and cross-shore components are
214 in good agreement with the observations. However, there are some differences between the observed and
215 simulated results; for example, the simulated ZMCC occupies a broader space than that in the
216 observations. This may have been caused by the relatively low number of observational stations.

217

Figure 3

219

220 Synoptic fluctuations of the TWC inshore branch during January and February 2009 were also validated
221 against the mooring results (Fig. 4). Since the TWC shows a strong signature at Station 4, the time series
222 of the alongshore currents and cross-shore currents in the whole water column of Station 4 were used for
223 the validation. To eliminate the influence of local effects, the simulated currents were averaged in a $10 \times$
224 10 km^2 area around Station 4. Both the observed and simulated results show that the TWC fluctuates
225 with a period of 3–15 days. The simulated TWC (Fig. 4a, warm color) appeared stronger ($> 0.1 \text{ m/s}$) on
226 Jan. 7, Jan. 12, Jan. 18, Jan. 21, Jan. 26, Jan. 29, Feb. 10, Feb. 14, Feb. 19, Feb. 22, and Feb. 25, which
227 agrees well with data from the observations (Fig. 4b). The time series of the simulated cross-shore
228 component (Fig. 4c) are virtually in phase with the observations (Fig. 4d). The magnitude of the cross-
229 shore fluctuations is comparable to the alongshore fluctuations. This is different~~in contrast~~ to the
230 anisotropic characteristic of~~feature for~~ the mean currents (Fig. 3), i.e., that for which the alongshore
231 component is nearly one order of magnitude larger than the cross-shore component ~~in the mean condition,~~
232 ~~the magnitude of the cross-shore fluctuations is comparable to the alongshore fluctuations.~~

233

234

Figure 4

235

236 2.3 EOF analysis of synoptic fluctuations

237 The Empirical Orthogonal Function (EOF) method (Emery and Thomson, 2001), as a statistical method,
238 has been used to understand synoptic fluctuations of the wintertime TWC. The simulated currents from
239 Jan. 1 to Feb. 28, 2009 were selected and their anomalies were calculated. Then, using the Matlab EOF-
240 function, the current vectors were separated into several orthogonal modes to show the spatial and

241 temporal variations. Because the first two leading modes explain 91 % of the total variance, only these
242 two modes were used for the analysis.

243

244 The spatial distributions of the two leading EOF modes were used to analyze the regional difference of
245 the synoptic fluctuations. To investigate the driving force of the two EOF modes, the temporal variation
246 was compared to the potential influence factors, such as wind, upstream currents, and net surface heat
247 flux.

248

249 **2.4 Momentum analysis**

250 The driving mechanisms of the synoptic fluctuations were further analyzed using the momentum
251 equation. First, the momentum balance as implemented in FVCOM (Chen et al., 2003) is shown in Eq.
252 (1). The three terms on the left hand side represent local acceleration, Coriolis acceleration, and advection,
253 respectively, and the three terms on the right hand side represent pressure gradient, friction, and diffusion,
254 respectively.

$$255 \quad \frac{\partial \bar{V}}{\partial t} - 2\bar{\Omega} \times \bar{V} + (\bar{V} \cdot \nabla) \bar{V} = -\frac{1}{\rho_0} \nabla P + \frac{\partial}{\partial z} \left(K_m \frac{\partial \bar{V}}{\partial z} \right) + \bar{F}, \quad (1)$$

256 where \bar{V} is velocity, $\bar{\Omega}$ is the Earth's rotation angular velocity, ρ_0 is the average density, P is
257 pressure, K_m is the vertical eddy viscosity coefficient, and \bar{F} is horizontal diffusion.

258

259 Second, according to the hydrostatic approximation used in FVCOM [as shown in Eq. (2)], the pressure
260 gradient is given as the product of density times the gravitational acceleration. This results in Eq. (3),
261 which indicates that pressure gradient can be decomposed into the effects of the barotropic and baroclinic

262 components, as shown in Eq. (4).

$$263 \quad \frac{\partial P}{\partial z} = \rho g, \quad (2)$$

$$264 \quad P_z = \int_z^\eta \rho g dz = \int_z^\eta (\rho_0 + \rho') g dz = \rho_0 g (z + \eta) + \int_z^\eta \rho' g dz, \quad (3)$$

$$265 \quad \nabla \vec{P} = \rho_0 g \nabla \eta + \nabla \left(\int_z^\eta \rho' g dz \right), \quad (4)$$

266 where ρ is density, ρ' is density anomaly, g is the gravitational acceleration, and η is sea surface
267 height.

268

269 Finally, the momentum equation is vertically integrated to estimate momentum balance for the water
270 column. Since the horizontal diffusion is a comparatively small term, it is neglected for simplicity.

$$271 \quad \int_{-H}^0 \frac{\partial \vec{V}}{\partial t} + \underbrace{\int_{-H}^0 -2\vec{\Omega} \times \vec{V}}_{\text{Coriolis}} + \underbrace{\int_{-H}^0 (V \cdot \nabla \vec{V})}_{\text{Advection}} = \underbrace{-gH \nabla \eta}_{\text{Barotropic}} - \underbrace{\int_{-H}^0 \nabla \left(\int_z^\eta \rho' g dz \right)}_{\text{Baroclinic}} + \underbrace{\rho_a C_D |\vec{U}| \vec{U}}_{\tau_a} - \underbrace{k_b |\vec{V}_b| \vec{V}_b}_{\tau_b}, \quad (5)$$

Total Pressure

272 where τ_a is wind stress and τ_b is bottom stress, ρ_a is the density of air, \vec{U} is the wind speed at 10
273 m above sea surface, C_D is a drag coefficient at the sea surface (which varies with wind speed \vec{U}),
274 k_b is a bottom friction coefficient ($k_b = 0.005$), and \vec{V}_b is the simulated velocity at the bottom.

275

276 3 Results

277 3.1 Mean distribution of TWC in winter

278 Since the observational results (Su and Pan, 1987; Zeng et al., 2012) show that both branches of the
279 wintertime TWC are flowing in the subsurface, we use the vertical maximum velocity (VMV) and its
280 corresponding depth as two indices to quantify the strength of the subsurface currents (Fig. 5).

281

282 As stated above, the distribution of the VMV shows two branches of the TWC (Fig. 5a). The inshore
283 branch (Fig. 5a, blue arrow of IB), which was located between the 30 and 100 m isobaths, followed a
284 straight route from the northwest of Taiwan to the northern ECS shelf. The offshore branch (Fig. 5a, blue
285 arrow of OB) existed near the 100 m isobath and had ~~a horizontal structure with~~ two meanders. The two
286 meanders turn to the cross-shore direction along latitudes 26.5°N and 28°N. These two branches are
287 further illustrated in the distributions of current speed along the six cross-TWC sections (S1-S6), which
288 were located at critical points in the two meanders (Fig. 6). From the VMV structure, it can be inferred
289 that the intrusions of the TSC and the Kuroshio Current both affected the origin of the offshore branch
290 (Fig. 6, S1-S3).

291

292 We further examined the subsurface current core using the depth of the VMV (Fig. 5b). We found that
293 the VMV of the TWC was located 40–60 m below the surface at the inshore branch and 20–40 m below
294 the surface at the offshore branch. Figure 6 shows the VMV positions in the subsurface layer; it also
295 illustrates that the depth of the subsurface VMV in the inshore branch was deeper than that in the offshore
296 branch. ~~The northerly wind in winter weakens the northward TWC, particularly in the upper layer, which~~
297 ~~leads to the formation of the subsurface VMV.~~ The difference can be explained by the combined effects
298 of baroclinicity and wind friction. Assuming a relatively spatially homogeneous heat loss, ~~a different~~
299 cooling occurs, due to the smaller heat capacity of the shallow coastal water compared to the deeper
300 offshore waters; hence generating a northwestward horizontal density gradient leading to a ~~southeastward~~
301 northeastward thermal current (vertical current shear) according to the thermal wind relationship,
302 resulting in an increasing of southwestward–northeastward flow ~~component from surface to~~
303 ~~bottom~~ increasing upward. ~~The northeasterly wind in winter weakens the northeastward TWC,~~

304 ~~particularly in the upper layer, which leads to the formation of the subsurface VMV, which in turn~~
305 ~~weakens the northeastward flow of the TWC inshore branch.~~ Therefore, the fact that the depth of the
306 subsurface current core in the inshore branch is greater than that in the offshore branch indicates that a
307 ~~weaker baroclinicity or a the effects of baroclinicity and wind~~stronger wind friction on the inshore branch
308 ~~are stronger than~~on the offshore branch.

309

310 The magnitude of the wintertime TWC was obtained by flux analysis. Two dividing lines (Fig. 5a, red
311 lines) were defined as the boundaries for the ZMCC, the TWC inshore branch, and the TWC offshore
312 branch, which had the weakest flows. The flux of each branch (Fig. 5c) was calculated using the
313 horizontal integration between the boundaries and the vertical integration in the water column. The
314 inshore branch intensifies along its way and becomes significant north of 26.5 °N, showing particularly
315 strong flow velocities between 27.5 and 28.0 °N. In this area, the subsurface current was much stronger
316 from S4 to S5 than in the other areas (Fig. 6). The flux in the entire offshore branch was large, particularly
317 north of Taiwan.

318

319

Figure 5

320

321

Figure 6

322

323 **3.2 Synoptic fluctuations**

324 The observations (Fig. 4) have demonstrated that the synoptic fluctuation in the TWC inshore branch
325 (near 121.5 °E, 27.0 °N) is significant. We further investigated the regional difference of fluctuations in

326 the two TWC branches in winter 2009 using the following three steps: (i) two regions with significant
327 fluctuations are identified by the current standard deviations of the VMV (Fig. 7) and the corresponding
328 temporal variation of vertical structures at their extremes (Fig. 8); (ii) each of the two significant
329 fluctuations is decomposed into EOF components (Fig. 9), and (iii) the influence factors, such as wind,
330 upstream currents, and net surface heat flux, are investigated by examining their correlations with the
331 first two leading EOF components (Figs. 10 and 11).

332

333 The current standard deviations (Fig. 7) shows that prominent fluctuations occurred in two regions: north
334 of Taiwan and the inshore area. The standard deviations of VMV at the two regions were larger than 0.1
335 m/s (comparable to the mean currents). In the area north of Taiwan, the fluctuation was located in the
336 origin area of the TWC offshore branch. The fluctuation in this region was in phase with the fluctuation
337 in the Taiwan Strait, indicating that the TSC played an important role in generating the fluctuation north
338 of Taiwan (to a greater extent than did the Kuroshio intrusion). The TWC fluctuation had a strong

339 ~~magnitude in the~~ cross-shore direction component, which means the fluctuation transported the water
340 north of Taiwan to both the inshore and offshore branches. In the inshore area, the fluctuations ~~was~~ were
341 influencing located in a wide region between the 30 and 100 m isobaths, with a magnitude sometimes
342 being larger than the mean flow (Fig. 5a). These strong fluctuations led to an episodic occurrence of the
343 TWC inshore branch, as observed at the site off the Zhe-Min coast (Fig. 4, high temperature). When the
344 TWC inshore branch was weakened due to these fluctuations, the ZMCC might even dominate a wide
345 region outside of the 100 m isobath, especially at the surface (Fig. 4, low temperature).

346 ~~where the southwestward flowing ZMCC and the northeastward directed TWC meet. As deduced from~~
347 ~~the standard deviation, the currents fluctuated significantly in the alongshore direction, indicating that~~

348 ~~the TWC inshore branch occurred episodically.~~

349

350  Figure 7

351

352 The vertical structures of the fluctuations north of Taiwan and in the inshore area at two representative
353 points and their relation with upper mixed layer depth are further analyzed (Fig. 8). The major component
354 (the alongshore current) of the TWC in each of the two regions (P1 and P2, Fig. 7) is used to show the
355 vertical structure of the fluctuation. The depths of the upper mixed layer were determined by a
356 Richardson number criterion (Mellor and Durbin, 1975; Grachev et al., 2013; Richardson et al., 2013),
357 i.e., where the critical Richardson number equals 0.25 in this paper [as in Xuan et al. (2012)]. The mean
358 depth of the upper mixed layer north of Taiwan (20 m) was much shallower than the mean depth in the
359 inshore area (42 m). However, the TWC (Fig. 8, warm color) fluctuated with significant variations of the
360 upper mixed layer depth (Fig. 8, gray lines) in both areas. When the upper mixed layer deepened, the
361 northeastward TWC (Fig. 8, warm color) was weakened or even replaced by the southwestward ZMCC,
362 and vice versa. ~~Hence, w~~Wind and surface cooling, which both drive the mixed layer depth, can affect
363 the TWC fluctuation.

364

365  Figure 8

366

367 The TWC fluctuations were further decomposed into EOF modes. The first two leading EOF modes
368 account for 54% and 37% of the total variances (Fig. 9), ~~which were~~ associated with the two prominent
369 fluctuations north of Taiwan and in the inshore area (Fig. 7). Both EOF modes had a maximum fluctuation

370 larger than 0.2 m/s (comparable to the mean currents). The spatial pattern of the first EOF mode (EOF1,
371 Fig. 9a) shows that the fluctuation continued from the Taiwan Strait to the area north of Taiwan,
372 indicating that the fluctuation north of Taiwan was related to the TSC and not to the Kuroshio Current.
373 The alongshore component also showed a strong fluctuation in the Taiwan Strait, which means that the
374 TSC episodically intruded the shelf. The cross-shore component revealed a ~~great~~ fluctuation north of
375 Taiwan that was larger than 0.1 m/s. This cross-shore fluctuation impacted on the trajectory of the TWS
376 water, synoptically flowing into the TWC inshore branch, offshore branch, or Kuroshio Current.

377

378 The spatial pattern of the second EOF mode (EOF2, Fig. 9b) shows a synoptic fluctuation in the inshore
379 area. ~~The fluctuation mainly varied in the alongshore direction, which indicates the episodic occurrence~~
380 ~~of the TWC inshore branch.~~ The area with alongshore fluctuation (Fig. 9d) larger than 0.1 m/s was located
381 between the 30 and 100 m isobaths, which demonstrates that the TWC could ~~also~~ episodically affect this
382 area. In addition, there were cross-shore fluctuations in the inshore area (Fig. 9f), mostly along the
383 latitudes 26.5°N and 28°N. The latitudes of ~~great~~ larger cross-shore fluctuations agreed well with the
384 latitudes where the TWC offshore branch of the mean currents (Fig. 5a) turned to the cross-shore
385 direction. This indicated that the cross-shore transports were most significant at the latitudes 26.5°N and
386 28°N, according to both the mean currents and the synoptic fluctuations.

387

388 Figure 10 shows the temporal variation of EOF1 and its relation with north-south component of wind
389 speed, net surface heat flux, the TSC, and the Kuroshio Current. We found a close correlation between
390 EOF1 and TSC ($R = 0.86$), demonstrating that the TSC played the most important role in generating the
391 TWC fluctuation north of Taiwan. The EOF1 and TSC were positively correlated, meaning that a larger

392 TSC intrusion north of Taiwan leads to a cross-shore current from the coastal area to the offshore area
393 and that a weak TSC intrusion causes a cross-shore current from offshore to inshore north of Taiwan.

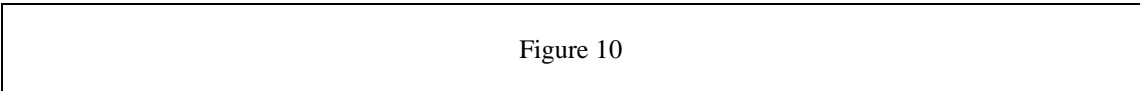
394

395 Figure 11 shows the temporal variation of EOF2 and its relation with the north-south component of wind
396 speed, net surface heat flux, the TSC, and the Kuroshio Current. It can be seen that EOF2 and wind are
397 well correlated ($R = 0.89$), indicating the important role of wind in generating the TWC fluctuation in
398 the inshore area. The ~~northerlynortheasterly~~ monsoon would greatly enhance the southwestward ZMCC,
399 which ~~would then~~ replaces the northeastward TWC in the inshore area. ~~Together with the effect of net~~
400 ~~surface heat flux, the stronger northerly monsoon during Jan. 5-13, Jan. 19-25 and Feb. 16-18 causes the~~
401 ~~deepening of the mixed layer (P2, Fig. 8).~~

402

403  Figure 9

404

405  Figure 10

406

407  Figure 11

408

409 3.3 Dynamic diagnostics

410 The wintertime (January and February 2009) mean of the water column momentum balance (Fig. 12) is
411 used to show the overall distribution of the fundamental forces over the ECS shelf. The Coriolis force
412 (Fig. 12a) is mainly balanced by the total pressure (Fig. 12b) in both branches, indicating the dominant

413 role of geostrophic balance in the wintertime TWC. However, the wind-induced surface friction plays an
414 important role in the TWC, especially in the inshore area and the Taiwan Strait (Fig. 12c). The bottom
415 friction has an impact north of Taiwan and in the shallow Taiwan Strait, in particular when significant
416 Kuroshio intrusion enhances the bottom flow (Fig. 12d). The effects of advection and acceleration are
417 predominantly local indicated by mostly incoherent small scale distributions (Figs. 12e, 12f), so they can
418 be ignored when studying the large-scale current of the wintertime TWC.

419

420

Figure 12

421

422 The variation of the driving forces at two representative points P1 and P2 were used to analyze the
423 dynamics of synoptic fluctuations north of Taiwan and in the inshore area. Regarding the results from
424 the EOF analysis, the three force terms, namely Coriolis, total pressure, and wind (Fig. 13), were selected
425 to investigate the effect of the TSC on the fluctuation north of Taiwan (Fig. 9a) and the effect of wind on
426 the fluctuation in the inshore area (Fig. 9b).

427

428 In the area north of Taiwan, the cross-shore fluctuations were induced by the TSC intrusion. The variation
429 of alongshore Coriolis force (Fig. 13a, black line) was much greater than the cross-shore Coriolis force
430 (Fig. 13b, black line), which means that the fluctuation north of Taiwan was mainly in the cross-shore
431 direction. The Coriolis force (Fig. 13a, black line) was mainly balanced by the total pressure (Fig. 13a,
432 blue line), which means the currents fluctuations north of Taiwan are dominated by geostrophic balance.
433 As mentioned in Sect. 3.2, the TWC fluctuation north of Taiwan was associated with the TSC rather than
434 with the Kuroshio Current. Therefore, in the shallow coastal area the TSC mainly caused variations in

435 the depth-independent barotropic pressure gradients, which further generated the cross-shore fluctuation.
436 The mechanism can be interpreted as follows. When a larger TSC intrusion occurred, the isobaric slope
437 tilted downward from south to north, generating a cross-shore current from the coastal area to the offshore
438 area. On the contrary, when the TSC intrusion was weak, the Kuroshio intrusion from offshore to inshore
439 dominated north of Taiwan.

440

441 Wind friction (Figs. 13c and 13d) was a fundamental factor in generating the fluctuations in the inshore
442 area. Although the geostrophic balance dominated in the inshore branch for most of the time, the
443 episodically strong winter monsoon had an important role in generating the TWC fluctuations. The
444 northwestward direction Coriolis force (Fig. 13c, black line) shows that the southwestward ZMCC
445 occurred on Jan. 12, Jan. 22, and Feb. 14, 2009 and was associated with a ~~northerly~~northeasterly wind
446 (Fig. 13c, red line). It indicates that strong ~~northerly~~northeasterly monsoon in winter can reduce or even
447 stop the northeastward TWC in the inshore area, causing the intermittency of the TWC inshore branch.

448

449

Figure 13

450

451 **4 Discussion**

452 ~~The s~~Simulated results in the winters (December-March) of the years 2010 to 2013 (Fig. 14) show that
453 general structures of the TWC in the other winters were similar to that in winter 2009 (Fig. 5 and Fig. 9),
454 which indicates that the results from the winter 2009 can be regarded as representative for the winter
455 situation. The two TWC branches and the two areas of strong fluctuations were presented ~~in the~~ all
456 winters from ~~of~~ 2009 to 2013, although their strength showed a certain inter-annual variability in

457 accordance with the changing surface forcing and boundary fluxes.

458

459

Figure 14

460

461 The wintertime TWC, which is manifested by ~~with~~ two subsurface branches and significant synoptic
462 fluctuations, has a very different structure when compared with the stationary and surface summertime
463 TWC reported in previous studies (Guan, 1978; Fang et al., 1991; Isobe, 2008). The synoptic events,
464 with time scales of 3-15 days, play a dominant role on the horizontal advective transports. According to
465 Ledwell et al. (1998) synoptic variations are much more effective on the horizontal transport than
466 variations on shorter time scales. The synoptic fluctuations modulate the spatial structure of the
467 wintertime TWC, especially when their magnitudes are comparable with that of the mean currents, such
468 as the two prominent fluctuations north of Taiwan and in the inshore area (Fig. 7). Therefore, the two
469 prominent fluctuations will be discussed next in terms of their contributions to the alongshore and cross-
470 shore transports.

471

472 **4.1 Cross-shore transport north of Taiwan induced by the TSC**

473 In the area north of Taiwan, the TSC intrusion generated strong fluctuations of the TWC in the cross-
474 shore direction (Fig. 9a). When a larger TSC intrusion occurred, the isobaric slope tilted downward from
475 south to north, generating a cross-shore current from the coastal area to the offshore area. Compared to
476 the reported summer route that transports Taiwan Strait water to the inshore area between the 30 and 100
477 m isobaths (Guan, 1978; Fang et al., 1991; Isobe, 2008; Yang et al., 2011, 2012), our results showed that
478 most Taiwan Strait water was transported to the TWC offshore branch and to the Kuroshio area as a result

479 of the cross-shore fluctuations induced by the synoptic TSC intrusion.

480

481 A numerical tracer simulation was used to analyze the role of the cross-shore fluctuation in the transport
482 of the TSC water and the Kuroshio water north of Taiwan. In order to demonstrate the characteristics of
483 the flow patterns more clearly, artificial tracers are released in the model domain and transported by the
484 velocity field provided by the FVCOM simulation. The tracer running was part of the FVCOM simulation;
485 therefore, all the above mentioned dynamics were involved, e.g., tide, wind, and boundary forces. The
486 release location and start date of the particles were configured as follows. Two sections, one in the Taiwan
487 Strait (Fig. 15a, black dots) and another in the East Taiwan Channel (Fig. 15b, black dots), were selected
488 as the source locations for the water masses of the TSC and the Kuroshio, respectively. The particles
489 were released on January 1, 2009 and tracked until March 31, 2009 (a total of 90 days).

490

491 Figure 15a shows the traces originating from the TSC area. Unlike the traditional route, where the TSC
492 water flows from the Taiwan Strait to the inshore area between the 30 and 100 m isobaths, most particles
493 (Fig. 15a, gray lines) were concentrated in the offshore branch under the effect of cross-shore fluctuation.
494 Two particles were selected to show the inshore route (Fig. 15a, red line) and offshore route (Fig. 15a,
495 blue line), with both passing the area north of Taiwan. When the two particles arrived at the area north
496 of Taiwan, the behavior of the tracers, according to specific velocity conditions (Fig. 15c), was very
497 different: a northwestward transport occurred on Jan. 25 for the inshore particles (Fig. 15c) and a
498 northeastward transport occurred on Feb. 12 for the offshore particles (Fig. 15c). The velocity conditions
499 in the area north of Taiwan corresponded to the variation of the Taiwan Strait flux (Fig. 10), which shows
500 that the Taiwan Strait flux on Feb. 12 was much greater than on Jan. 25. Therefore, it can be concluded

501 that the TSC intrusion induced an offshore transport north of Taiwan.

502

503 Figure 15b shows the traces originating from the Kuroshio area. In the same way as the TSC water, the

504 Kuroshio water was also transported to the northern shelf via both the inshore branch and the offshore

505 branch. The separation of the two branches north of Taiwan was caused by cross-shore fluctuations of

506 the currents. When the two particles arrived at the area north of Taiwan, a northwestward transport

507 occurred on Feb. 2 for the inshore particles (Fig. 15c) and a northeastward transport occurred on Feb. 12

508 for the offshore particles (Fig. 15c). This means that the offshore transport induced by the TSC also had

509 an effect on the distribution of Kuroshio water north of Taiwan. Liu et al. (2016) showed that the winter

510 TSC originated from a small branch of Kuroshio intrusion into the Luzon Strait. Our results complement

511 this picture, since they show that most TSC particles flow into the TWC offshore branch under the

512 influence of cross-shore fluctuation.

513

514

Figure 15

515

516 Our results may underestimate the impact of Kuroshio intrusion on the fluctuation of the TWC northeast

517 of Taiwan, especially at the seasonal and interannual time scales. Wei et al. (2013) demonstrated that the

518 annual and interannual variations of the Kuroshio volume transport are large. In addition, Zhou et al.

519 (2015) pointed out that the annual and interannual variations of the Kuroshio intrusion northeast of

520 Taiwan are prominent. Liu et al. (2014b) presented supportive evidence that the Kuroshio intrusion, from

521 east of Taiwan to the onshore area north of Taiwan, is closely related to the Kuroshio volume transport.

522 This relation between the Kuroshio intrusion and the Kuroshio volume transport had been interpreted by

523 Su and Pan (1987) as the β -effect because of the sudden change in topography northeast of Taiwan. Our
524 results show that the intra-seasonal variation of the Kuroshio intrusion and the Kuroshio volume transport
525 was negligible compared with the TSC variation at the same time scale, indicating that the synoptic
526 fluctuation of TWC north of Taiwan is mainly induced by the TSC. However, because FVCOM uses
527 sigma co-ordinates in the vertical which are prone to errors in regions of steep topography, our results
528 may underestimate the fluctuations at the shelf break, in particular to the northeast of Taiwan where
529 Kuroshio intrusion occurs.

530

531 **4.2 Water exchange in the inshore area induced by wind**

532 In the inshore area, the synoptic fluctuations of the TWC (Fig. 9b) caused by wind were generally strong
533 in the alongshore direction and regionally important (along the latitudes 26.5° N and 28° N) in the cross-
534 shore direction. The alongshore fluctuations showed that the TWC inshore branch occurred episodically.
535 This episodic occurrence of the TWC agrees with the results from a previous study based on four mooring
536 surveys off the Zhe-Min coast (Zeng et al., 2012). The mechanism of the episodic occurrence of the TWC
537 was mainly associated with the winter monsoon, which agrees with the analysis of observational data by
538 Huang et al. (2016). However, the overall magnitude of the TWC fluctuation, and its role on the cross-
539 shore flux, are still not fully understood due to the short-term nature of the observational data.

540

541 We investigated the magnitude of TWC fluctuation, and its role on the water exchange, in the inshore
542 area. Previous studies (Su and Pan, 1987; Zeng et al., 2012) show that the TWC flows between the 50
543 and 100 m isobaths, whereas the ZMCC water dominates the coastal area west of the 50 m isobath in the
544 surface layer. As mentioned when discussing Figure 9d, the strongest TWC could reach the coastal area

545 as close as the 30 m isobath, being stronger than those reported in the literature. Moreover, the area with
546 large fluctuations spanned the area between the 30 and 100 m isobaths (Fig. 9b), indicating that water
547 ~~exchange between the ZMCC water and the TWC water exists in the area between the 30 and 100 m~~
548 ~~isobaths between the 30 and 100 m isobaths may be either ZMCC or TWC water.~~

549

550 The episodic occurrence of the TWC inshore branch is directly related to the relative importance of the
551 southwestward ZMCC (Fig. 16, blue arrows) and the northeastward TWC (Fig. 16, red arrows). In this
552 paper, only wind-induced synoptic fluctuations are considered, ~~in the relations to the episodic events and~~
553 ~~no~~ not short-term extreme storm events. When the winter monsoon (the ~~northerly~~ northeasterly wind)
554 prevails, the ZMCC occupies most of the inshore area and the TWC inshore branch weakens (Fig. 16a).

555 On the contrary, the TWC inshore branch can intrude into the near-coast area under south westerly wind
556 conditions (Fig. 16b). The boundary between the coastal current and the TWC may shift from the 100 m
557 isobaths to the 30 m isobath in the cross-shore direction, covering the entire area of the TWC inshore
558 branch.

559

560 Our results further reveal that strong wind-induced cross-shore fluctuations occur in the inshore area (Fig.
561 9f). This cross-shore fluctuation has a significant ecological impact because of the connected nutrient
562 transport (Zhao and Guo, 2011). Ren et al. (2015) observed a cross-shore flux in the inshore area, which
563 was triggered by the transition of northeasterly to southwesterly ~~monsoonal~~ winds. Their observed
564 features can be further interpreted with our result that wind-induced fluctuations can affect the cross-
565 shore water transport in the inshore area.

566

567 Largest cross-shore fluctuations were located at the latitudes 26.5 °N and 28 °N (Fig. 9f), which agreed
568 well with the latitudes where the TWC offshore meanders occurred in the mean currents (Fig. 5a). ~~This~~
569 ~~also indicates that~~ Thus the offshore transports were most significant along the latitudes 26.5 °N and 28 °N
570 according to both the mean currents and the synoptic fluctuations. The offshore transport may be
571 associated with the offshore-penetrating fronts of coastal water in the ECS. Many remote-sensing images
572 (He et al. 2010; Bai et al. 2013) have exhibited offshore-penetrating fronts that crossed the 70 m isobath
573 and played an important role in cross-shore material exchange, but the mechanisms of the offshore-
574 penetrating fronts are still under debate. Yuan and Qiao (2005) pointed out that both downwelling- and
575 upwelling-favorable winds are associated with the occurrence of the offshore-penetrating front. Ren et
576 al. (2015) suggested that the penetrating front is generated by the transition of northeasterly to
577 southwesterly ~~monsoonal~~ winds. Wu (2015) suggested that the offshore-penetrating front is the response
578 of buoyant coastal water to an along-isobath undulation of the ambient pycnocline, which is controlled
579 by a temperature stratification of the water column. Our study offers a new interpretation, i.e., that the
580 penetrating front is generated through the wind-induced fluctuations and the TWC offshore meanders.

581

582

583

Figure 16

584

585 **5 Conclusions**

586 The FVCOM model was able to reproduce the wintertime TWC in 2009 reasonably well, as shown by a
587 validation in terms of the overall structure of the surface mean currents, the ECS boundary fluxes, and
588 data from four mooring stations. The validation showed that the simulated TWC was comparable to the

589 observed results, not only in terms of the mean currents but also in terms of the synoptic fluctuations.

590

591 The wintertime TWC showed two branches: one inshore and another offshore. The inshore branch

592 covered an area between the 30 and 100 m isobaths and flowed northeastward via a straight route. The

593 offshore branch was located between the 100 and 200 m isobaths and showed two prominent meanders.

594 It was shown that the Coriolis force was nearly balanced by the pressure gradient in both branches,

595 indicating the dominant role of the geostrophic balance for the mean current in both branches.

596

597 Two regions with significant synoptic fluctuations, north of Taiwan and the inshore area, were

598 investigated using the EOF method. The first two leading modes explained 91% of the total variance.

599 EOF1 showed that fluctuations occurred in the cross-shore direction south of 26 °N. These fluctuations

600 were mainly associated with variation of the TSC flux. EOF2 showed significant fluctuation between the

601 30 and 100 m isobaths. These fluctuations caused the episodic existence of the TWC inshore branch in

602 the alongshore direction and cross-shore fluctuations mainly at latitudes 26.5 °N and 28 °N, which were

603 mainly associated with the variation of wind speed.

604

605 We also studied the different dynamic reasons for the fluctuations in the two regions. In the area north of

606 Taiwan, the TSC and Kuroshio converged to initiate the TWC. A barotropic pressure anomaly was

607 generated by TSC intrusion from the Taiwan Strait causing a barotropic pressure gradient in the

608 alongshore direction; this explains why the synoptic fluctuations in this area occurred in the cross-shore

609 direction. Additionally, the wind had a strong effect on the synoptic fluctuations in the inshore area. The

610 northeasterly monsoon enhanced the southwestward ZMCC and replaced the TWC in the inshore area.

611 This situation is reversed during the southwesterly monsoonwind.

612

613 The synoptic fluctuations north of Taiwan and in the inshore area are important for both the alongshore
614 and cross-shore transports. Due to the fluctuation north of Taiwan, the mixed water of the TSC and the
615 Kuroshio was transported to both the inshore area and the offshore area, whereas most Taiwan Strait
616 water was transported to the offshore area in winter. The inshore fluctuation not only caused an episodic
617 occurrence of the TWC in the alongshore direction, which affected the alongshore transport of ZMCC
618 water and TWC water between the 30 and 100 m isobaths, but also impacted the cross-shore transports
619 along latitudes 26.5°N and 28°N.

620

621 **Acknowledgement**

622 The authors sincerely thank Dr. John M. Huthnance and the three anonymous reviewers for insightful
623 suggestions that improved this manuscript. This study was jointly supported by the Sino-German
624 cooperation in ocean and polar research under the grant BMBF-03F0701A (CLIFLUX), the National
625 Natural Science Foundation of China (~~41306025, 41276028, 41321004~~U1609201), the grant from the
626 scientific research fund of the Second Institute of Oceanography, SOA (QNYC201603) and the project
627 of State Key Laboratory of Satellite Ocean Environment Dynamics, the Second Institute of
628 Oceanography (SOEDZZ1512).

629

630 **References**

631

632 Bai, Y., Pan, D., Cai, W. J., He, X., Wang, D., Tao, B., and Zhu, Q.: Remote sensing of salinity from
633 satellite-derived CDOM in the Changjiang River dominated East China Sea, *J. Geophys. Res. Ocean*,
634 118, 227–243, 2013.

635 Bleck, R.: An oceanic general circulation model framed in hybrid isopycnic-Cartesian coordinates,
636 *Ocean Model.*, 37, 55–88, 2002.

637 Brink, K. H.: Costal trapped waves and wind-induced currents over the continental shelf, *Annual Review*
638 *of Fluid Mechanics*, 23, 389–412, 1991.

639 Carnes, M. R.: Description and evaluation of GDEM-V3.0, NRL Rep. NRL/MR/7330-09-9165, Nav.
640 Res. Lab., Washington, D. C., 2009.

641 Chen, C., Liu, H., and Beardsley, R. C.: An unstructured, finite-volume, three-dimensional, primitive
642 equation ocean model: application to coastal ocean and estuaries, *J. Atm. Oceanic Tech.*, 20, 159–
643 186, 2003.

644 Chen, C., Beardsley, R. C., Limeburner, R., and Kim, K.: Comparison of winter and summer
645 hydrographic observations in the Yellow and East China seas and adjacent Kuroshio during 1986,
646 *Cont. Shelf Res.*, 14, 909–929, 1994.

647 Chen, C., Xue, P., Ding, P., Beardsley, R. C., Xu, Q., Mao, X., Gao, G., Qi, J., Li, C., Lin, H., Cowles,
648 G., and Shi, M.: Physical mechanisms for the offshore detachment of Changjiang Diluted Water in
649 the East China Sea, *J. Geophys. Res.*, 113, C02002, doi:10.1029/2006JC003994, 2008.

650 Chen, C. T. A. and Wang, S. L.: Carbon, alkalinity and nutrient budget on the East China Sea continental
651 shelf, *J. Geophys. Res. Ocean*, 104, 20675–20686, 1999.

652 Chuang, W. S. and Liang, W. D.: Seasonal variability of intrusion of the Kuroshio water across the
653 continental shelf northeast of Taiwan, *J. Oceanogr.*, 50(5), 531–542, 1994.

654 Cui, M., Hu, D., and Wu, L.: Seasonal and intraseasonal variations of the surface Taiwan Warm Current,
655 *Chin. J. Oceanol. Limnol.*, 22, 271–277, 2004.

656 Egbert, G. D., Bennett, A., and Foreman, M.: TOPEX/Poseidon tides estimated using a global inverse
657 model, *J. Geophys. Res.* 99, 24821–24852, doi: 10.1029/94JC01894, 1994.

658 Egbert, G. D. and Erofeeva, S. Y.: Efficient inverse modeling of barotropic ocean tides, *J. Atmos. Oceanic*
659 *Technol.*, 19, 183–204, 2002.

660 Emery, W. J. and Thomson, R. E.: Data analysis methods in physical oceanography, Second and revised
661 version, 658 pp., Elsevier Science B.V., Amsterdam, The Netherland, 2001.

662 Fang, G., Zhao, B., and Zhu, Y.: Water volume transport through the Taiwan Strait and the continental
663 shelf of the East China Sea measured with current meters, in *Oceanography of Asian Marginal Seas*,
664 edited by K. Takano, 345–358pp., doi:10.1016/S0422-9894(08)70107-7, Elsevier, New York, 1991.

665 Feng, M., Mitsudera, H., and Yoshikawa, Y.: Structure and Variability of the Kuroshio Current in Tokara
666 Strait, *J. Phys. Oceanogr.*, 30(9), 2257–2276, 2000.

667 Godin, G.: *The Analysis of Tides*, 264 pp., University of Toronto Press, Toronto, 1972.

668 Grachev, A. A., Andreas, E. L., Fairall, C. W., Guest, P. S., and Persson, P. O. G.: The critical Richardson
669 number and limits of applicability of local similarity theory in the stable boundary layer, *Boundary-*
670 *layer meteorology*, 147(1), 51–82, 2013.

671 Guan, B. and Fang, G.: Winter counter-wind currents off the southeastern China coast: A review, *J.*
672 *Oceanogr.*, 62, 1–24, 2006.

673 Guan, B. and Mao, H.: A note on circulation of the East China Sea, *Chin. J. Oceanol. Limnol.*, 1, 5–16,
674 1982.

675 Guan, B. X.: A sketch of the current system of the East China Sea, in *Collected Papers of the Continental*
676 *Shelf of the East China Sea (in Chinese)*, 126–133pp., Inst. of Oceanol., Chin. Acad. of Sci.,
677 Qingdao, China, 1978.

678 Guo, X. Y., Hukuda, H., Miyazawa, Y., and Yamagata, T.: A triply nested ocean model for simulating the

679 Kuroshio - Roles of horizontal resolution on JEBAR, *J. Phys. Oceanogr.*, 33, 146–169, 2003.

680 Guo, X. Y., Miyazawa, Y., and Yamagata, T.: The Kuroshio onshore intrusion along the shelf break of
681 the East China Sea: The origin of the Tsushima Warm Current, *J. Phys. Oceanogr.*, 36, 2205–2231,
682 doi:10.1175/JPO2976.1, 2006.

683 He, L., Li, Y., Zhou, H., and Yuan, D.: Variability of cross-shelf penetrating fronts in the East China Sea,
684 *Deep Sea Res.*, 57, 1820–1826, 2010.

685 Hong, H., Chai, F., Zhang, C., Huang, B., Jiang, Y., and Hu, J.: An overview of physical and
686 biogeochemical processes and ecosystem dynamics in the Taiwan Strait, *Cont. Shelf Res.*, 31, 3-12,
687 2011.

688 Hsin, Y. C., Qiu, B., Chiang, T. L., and Wu, C. R.: Seasonal to interannual variations in the intensity and
689 central position of the surface Kuroshio east of Taiwan, *J. Geophys. Res. Oceans*, 118(9), 4305–
690 4316, 2013.

691 Hu, J., Kawamura, H., Li, C., Hong, H., and Jiang, Y.: Review on current and seawater volume transport
692 through the Taiwan Strait, *J. Oceanogr.*, 66, 591-610, 2010.

693 Huang, D., Zeng, D., Ni, X., Zhang, T., Xuan, J., Zhou, F., Li, J., and He, S.: Alongshore and cross-shore
694 circulations and their response to winter monsoon in the western East China Sea, *Deep-Sea Res. II*,
695 124, 6–18, <http://dx.doi.org/10.1016/j.dsr2.2015.01.001i>, 2016,

696 Hung, J. J., Chen, C. H., Gong, G. C., Sheu, D. D., and Shiah, F. K.: Distributions, stoichiometric patterns
697 and cross-shelf exports of dissolved organic matter in the East China Sea, *Deep-Sea Res. II*, 50,
698 1127–1145, 2003.

699 Huthnance, J. M., Mysak, L. A., and Wang, D. P.: Coastal trapped waves, in: Mooers C.N.K. (ed.)
700 Baroclinic Processes on Continental Shelves. *Coastal and Estuarine Sciences*, 3, pp. 1-18.
701 Washington DC, American Geophysical Union, 1986.

702 Huyer, A.: Shelf circulation, In Mehaute, B. L., Hames, D. M. (Eds.), *The Sea, Volume 9: Ocean*
703 *Engineering Science*, Wiley, pp. 423–466, 1990.

704 Isobe, A.: Recent advances in ocean-circulation research on the Yellow Sea and East China Sea shelves,
705 *J. Oceanogr.*, 64, 569–584, doi:10.1007/s10872-008-0048-7, 2008.

706 Johns, W. E., Lee, T. N., Zhang, D., Zantopp, R., Liu, C. T., and Yang, Y.: The Kuroshio east of Taiwan:
707 Moored transport observations from the WOCE PCM-1 array, *J. Phys. Oceanogr.*, 31(4), 1031–1053,
708 2001.

709 Ledwell, J. R., Watson, A. J., and Law, C. S.: Mixing of a tracer in the pycnocline, *J. Geophys. Res.*,
710 103(C10), 21499–21529, doi:10.1029/98JC01738, 1998.

711 Lee, J. S. and Matsuno, T.: Intrusion of Kuroshio water onto the continental shelf of the East China Sea,
712 *J. Oceanogr.*, 63, 309–325, 2007.

713 Liu, C., Wang, F., Chen, X., and VonStorch, J. S.: Interannual variability of the Kuroshio onshore
714 intrusion along the East China Sea shelf break: Effect of the Kuroshio volume transport, *J. Geophys.*
715 *Res. Oceans*, 119, 6190–6209, doi:10.1002/2013JC009653, 2014a.

716 Liu, T., Xu, J., He, Y., Lü H., Yao, Y., and Cai, S.: Numerical simulation of the Kuroshio intrusion into
717 the South China Sea by a passive tracer, *Acta Oceanologica Sinica*, 35(9): 1–12, doi:
718 10.1007/s13131-016-0930-x, 2016.

719 Liu, X., Dong, C., Chen, D., and Su, J.: The pattern and variability of winter Kuroshio intrusion northeast
720 of Taiwan, *J. Geophys. Res. Oceans*, 119, 5380–5394, DOI 10.1002/2014JC009879, 2014b.

721 Mellor, G. L. and Durbin, P A.: The structure and dynamics of the ocean surface mixed layer, *J. Phys.*
722 *Oceanogr.*, 5(4), 718–728, 1975.

- 723 Oey, L. Y., Hsin, Y. C., and Wu, C. R.: Why does the Kuroshio northeast of Taiwan shift shelfward in
724 winter?, *Ocean Dynam.*, 60(2), 413–426, 2010.
- 725 Qiu, B. and Imasato, N.: A numerical study on the formation of the Kuroshio countercurrent and the
726 Kuroshio Branch Current in the East China Sea, *Cont. Shelf Res.*, 10, 165–184, doi:10.1016/0278-
727 4343(90)90028-K, 1990.
- 728 Ren, J. L., Xuan, J., Wang, Z. W., Huang, D., and Zhang, J.: Cross-shelf transport of terrestrial Al
729 enhanced by the transition of northeasterly to southwesterly monsoon wind over the East China Sea,
730 *J. Geophys. Res. Oceans*, 120, doi:10.1002/2014JC010655, 2015.
- 731 Richardson, H., Basu, S., and Holtslag, A. A. M.: Improving stable boundary-layer height estimation
732 using a stability-dependent critical bulk Richardson number, *Boundary-layer meteorology*, 148(1),
733 93–109, 2013.
- 734 Smith, W. H. F. and Sandwell, D. T.: Global sea floor topography from satellite altimetry and ship depth
735 soundings, *Science*, 277, 1956–1962, 1997.
- 736 Su, J. L. and Pan, Y. Q.: On the shelf circulation north of Taiwan, *Acta Oceanol. Sin.*, 6, 1–20, 1987.
- 737 Su, J. L., Pan, Y. Q., and Liang, X. S.: Kuroshio intrusion and Taiwan warm current, *Oceanology of*
738 *China Seas*. Springer Netherlands, 59–70, 1994.
- 739 Takahashi, D. and Morimoto, A.: Mean field and annual variation of surface flow in the East China Sea
740 as revealed by combining satellite altimeter and drifter data, *Prog. Oceanogr.*, 111, 125–139, doi:
741 10.1016/j.pocean.2013.01.007, 2013.
- 742 Teague, W., Jacobs, G., Ko, D., Tang, T., Chang, K. I., and Suk, M. S.: Connectivity of the Taiwan, Cheju,
743 and Korea straits, *Cont. Shelf Res.*, 23(1), 63–77, 2003.
- 744 Uppala, S. M., Kållberg, P. W., Simmons, A. J., Andrae, U., Bechtold, V. D. C., Fiorino, M., Gibson, J.
745 K., Haseler, J., Hernandez, A., Kelly, G. A., Li, X., Onogi, K., Saarinen, S., Sokka, N., Allan, R. P.,
746 Andersson, E., Arpe, K., Balmaseda, M. A., Beljaars, A. C. M., Berg, L. V. D., Bidlot, J., Bormann,
747 N., Caires, S., Chevallier, F., Dethof, A., Dragosavac, M., Fisher, M., Fuentes, M., Hagemann, S.,
748 Hólm, E., Hoskins, B. J., Isaksen, I., Janssen, P. A. E. M., Jenne, R., McNally, A. P., Mahfouf, J.-F.,
749 Morcrette, J.-J., Rayner, N. A., Saunders, R. W., Simon, P., Sterl, A., Trenberth, K. E., Untch, A.,
750 Vasiljevic, D., Viterbo, P., and Woollen, J.: The ERA-40 re-analysis, *Q. J. R. Meteorol. Soc.*, 131,
751 2961–3012. doi:10.1256/qj.04.176, 2005.
- 752 Wang, Y., Jan, S., and Wang, D.: Transports and tidal current estimates in the Taiwan Strait from
753 shipboard ADCP observations (1999–2001), *Estuarine Coastal Shelf Sci.*, 57(1), 193–199, 2003.
- 754 Wei, Y., Huang, D., and Zhu, X. H.: Interannual to decadal variability of the Kuroshio Current in the east
755 china sea from 1955 to 2010 as indicated by in-situ hydrographic data, *J. Oceanogr.*, 69(5), 571–
756 589, 2013.
- 757 Wu, H.: Cross-shelf penetrating fronts: A response of buoyant coastal water to ambient pycnocline
758 undulation, *J. Geophys. Res.*, 120, doi:10.1002/2014JC010686, 2015.
- 759 Wu, C. R. and Hsin, Y. C.: Volume transport through the Taiwan Strait: a numerical study, *Terr. Atmos.*
760 *Ocean. Sci.*, 16(2), 377–391, 2005.
- 761 Xuan, J., Huang, D., Zhou, F., Zhu, X. H., and Fan, X.: The role of wind on the detachment of low salinity
762 water in the Changjiang Bank in summer, *J. Geophys. Res. Ocean*, 117, C10004, doi:
763 10.1029/2012JC008121, 2012.
- 764 Xuan, J., Yang, Z., Huang, D., Wang, T., and Zhou, F.: Tidal residual current and its role in the mean flow
765 on the Changjiang Bank, *J. Mar. Syst.*, 154, 66–81, doi: 10.1016/j.jmarsys.2015.04.005, 2016.
- 766 Xuan, J., Zhou, F., Huang, D., Zhu, X. H., Xing, C., and Fan, X.: Modelling the timing of major spring

767 bloom events in the central Yellow Sea, *Estuarine Coastal Shelf Sci.*, 113, 283–292, 2012.

768 Yang, D., Yin, B., Liu, Z., and Feng, X.: Numerical study of the ocean circulation on the East China Sea
769 shelf and a Kuroshio bottom branch northeast of Taiwan in summer, *J. Geophys. Res. Ocean*, 116,
770 C05015, doi:10.1029/2010JC006777, 2011.

771 Yang, D., Yin, B., Liu, Z., Bai, T., Qi, J., and Chen, H.: Numerical study on the pattern and origins of
772 Kuroshio branches in the bottom water of southern East China Sea in summer, *J. Geophys. Res.*
773 *Ocean*, 117, C02014, doi:10.1029/2011JC007528, 2012.

774 Yu, L. and Weller, R. A.: Objectively Analyzed air–sea heat Fluxes (OAFlux) for the global oceans, *B.*
775 *Am. Meteorol. Soc.* 88, 527–539, 2007.

776 Yuan, D., Qiao, F., and Su, J.: Cross-shelf penetrating fronts off the southeast coast of China observed by
777 MODIS. *Geophys. Res. Lett.*, 32, L19603, doi:10.1029/2005GL023815, 2005.

778 Zeng, D. Y., Ni, X., and Huang, D.: Temporal and spatial variability of the Zhe-Min Coastal Current and
779 the Taiwan Warm Current in winter in the southern Zhejiang coastal sea, *Sci. Sin. Terrae.*, 42, 1123–
780 1134, 2012.

781 Zhao, L. and Guo, X.: Influence of cross-shelf water transport on nutrients and phytoplankton in the East
782 China Sea: A model study, *Ocean Sci.*, 7, 27–43, doi:10.5194/os-7-27-2011, 2011.

783 Zhou, F., Xue, H., Huang, D., Xuan, J., Ni, X., Xiu, P., and Hao, Q.: Cross shelf exchange in the shelf of
784 the East China Sea, *J. Geophys. Res. Oceans*, 120, 1545–1572, doi:10.1002/2014JC010567, 2015.

785 Zhu, J., Chen, C., Ding, P., Li, C., and Lin, H.: Does the Taiwan Warm Current exist in winter?, *Geophys.*
786 *Res. Lett.*, 31, L12302, doi:10.1029/2004GL019997, 2004.

787 **Table Captions**

788 Table 1: Annual-mean volume transports ($S_v = 10^6 \text{ m}^3/\text{s}$) through various sections. The sections are
789 shown in Figure 2 using blue dashed lines.

790

791 **Figure Captions**

792 Figure 1: Density (σ_t , kg/m^3) distributions at 50 m depth derived from the GDEM climatological data in
793 February (a), an ocean survey from Feb. 1–27, 2007 (b), and an ocean survey from Feb. 3–16, 2007 (c),
794 with the density anomalies between the GDEM data and the two surveys (d and e). The two blue arrows
795 indicate the two TWC branches in winter. The 30, 50, 70, 100 and 200 m isobaths are indicated with grey
796 lines in panel a.

797

798 Figure 2: The FVCOM model grid (Left) and the surface mean flow in the ECS in winter (Right). The

799 colors in the left panel show the grid length (km). The letters a, b, and c indicate the three open boundaries
800 at the Taiwan Strait, the northwest Pacific Ocean, and the Japan/East Sea, respectively. The blue dashed
801 lines (right) show some important straits around shelf boundary, including the Taiwan Strait (TWS), the
802 East Taiwan Channel (ET), the Tsushima Strait (TUS), the Tokara Strait (TOS), and shelf break at the
803 200 m isobath. The red rectangle shows the study area of the wintertime TWC. The four red numbers off
804 the Zhe-Min coast shows the four mooring sites observed from Jan. 5 to Feb. 28, 2009.

805

806 Figure 3: Validations of the wintertime TWC (warm color) along the section off the Zhe-Min coast (the
807 short line with four red numbers in Figure 2): (a) observed alongshore currents; (b) simulated alongshore
808 currents; (c) observed cross-shore currents; (d) simulated cross-shore currents. Note, an enlarged color
809 scale is used for the cross-shore component to have a clear view of its weak structure.

810

811 Figure 4: Validations of the wintertime TWC fluctuations: (a) observed alongshore currents; (b)
812 simulated alongshore currents; (c) observed cross-shore currents; (d) simulated cross-shore currents. The
813 observation data comes from Station 4 in Figure 1 and the simulated data has the same position and
814 period as the observation data.

815

816 Figure 5: a) Distribution of flow axes in the ECS in winter. The black arrows show the maximum velocity
817 (m/s) in the vertical profile (VMV) and the color shows the speed of the VMV. The two blue arrows with
818 label IB and OB represent the flow axes of the inshore branch and offshore branch, respectively. The red
819 line DL1 represents the dividing line between the coastal current and inshore branch, and the red line

820 DL2 separates the two TWC branches. b) Depth (m) of flow axes in the ECS, shown by color. Sections

821 S1–S6 were selected to study the wintertime TWC. c) Flux of inshore branch (blue) and offshore branch
822 (red) at different latitudes. Dashed lines show the positions of Sections. S1–S6. Note, the scale is not
823 linear.

824

825 Figure 6: Distributions of current speed along the six sections S1–S6 in winter. The blue arrow on the
826 left indicates the inshore branch according to the velocity cores from section S3 to S6. The blue arrow
827 on the right indicates the offshore branch according to the velocity cores from section S2 to S6. TSC is
828 the Taiwan Strait Warm Current.

829

830 Figure 7: Current standard deviation (black arrows) in the layer of the VMV. The color shading shows
831 the magnitude of the current standard deviation. The two blue arrows indicate the two TWC branches.
832 The red curve indicate the area where the current standard deviation is larger than 0.1 m/s and ~~their~~ the
833 branches' representative points (P1 and P2) are selected for later analysis.

834

835 Figure 8: Variation of alongshore currents (m/s, shown by color scale) for the entire water column north
836 of Taiwan (P1) and in the inshore area (P2) and their relation with upper mixed layer depth. The positive
837 velocity (warm color) indicates the occurrence of the TWC. The gray solid lines show the depth of the
838 upper mixed layer.

839

840 Figure 9: The spatial pattern of the first (EOF1; left) and second (EOF2; right) leading modes of the
841 VMV in the ECS: (a) EOF1 currents, (b) EOF2 currents, (c) EOF1 alongshore component, (d) EOF2
842 alongshore component, (e) EOF1 cross-shore component, and (f) EOF2 cross-shore component (all

843 shown by black arrows with the color representing the magnitude). The 30, 50, 70, 100 and 200 m
844 isobaths are indicated with grey lines.

845

846 Figure 10: Temporal variation of EOF1, north-south component of wind speed, surface net heat flux, and
847 TSC flux along-across the TWS section, and Kuroshio flux along-across the ET section. Their linear
848 correlation coefficients R and time-lags are also indicated in each panel. The p value is a declining
849 indicator which indicates the impact significance of the linear correlation coefficients R whereby R has
850 statistical significance and the confidence level is larger than 95% when the p value is less than 0.05.

851

852 Figure 11: Temporal variation of EOF2, north-south component of wind speed, surface net heat flux, and
853 TSC flux along-across the TWS section, and Kuroshio flux along-across the ET section. Their linear
854 correlation coefficients and time-lags are also indicated in each panel.

855

856 Figure 12: The effects of Coriolis force (a), total pressure (b), surface friction (c), bottom friction (d),
857 advection (e), and local acceleration (f) for water column in winter according to Eq. (5) (shown by black
858 arrows with the color representing the magnitude; units: $10^{-4} \text{ m}^2/\text{s}^2$). The two blue arrows indicate the
859 two TWC branches. The two triangles indicate the two regions with significant fluctuation north of
860 Taiwan (P1) and in the inshore area (P2).

861

862 Figure 13: Variations in Coriolis force, total pressure, and wind in the alongshore direction at P1 (a), the
863 cross-shore direction at P1 (b), the alongshore direction at P2 (c), and the cross-shore direction at P2 (d)
864 according to Eq. (5).

865

866 Figure 14: Mean currents (upper panels) and synoptic fluctuations (EOF1 in middle panels and EOF2 in
867 bottom panels) in winters of 2010-2013. The black arrows in the upper panels show the velocity (m/s) in
868 the layer of VMV ~~and with~~ the color representing shows the current speed. The two blue arrows with
869 label IB and OB represent the flow axes of the inshore branch and offshore branch, respectively. The
870 black arrows in the middle panels and bottom panels represent the EOF components (m/s) with their
871 magnitude represented by color scales.

872

873 Figure 15: Traces of TSC water (a) and Kuroshio water (b) in winter, with the variation of surface currents
874 ~~at the original location of P1~~ north of Taiwan (c). The green lines L1 and L2 indicate the starting latitude
875 of the tracers (24.5°N) and the latitude which is representative for synoptic fluctuations north of Taiwan
876 (25.8°N), respectively. The black dots represent the release locations of tracers originated from line L1.

877 The gray lines show the entire trajectories of the tracers. The red lines and blue lines are selected
878 trajectories, which are close to the inshore branch and offshore branch, respectively. The dates show the
879 times ~~when that~~ selected tracers cross the latitude indicated by line L2, reached the origin location P1;
880 ~~note that the location of P1 is not fixed but varies with time.~~ The numbers are the depths of the tracers,

881 which are labeled at an interval of six days. The two black arrows represent the two TWC branches.

882

883 Figure 16: The VMV under the northerly wind (a) and southerly wind (b). Panel (c) shows the variation
884 of wind in winter. Blue vectors and red vectors show the southwestward coastal current and the
885 northeastward TWC, respectively. Gray contours indicate the 30, 50, 70, and 100 m isobaths. The two
886 black arrows represent the two TWC branches. The green ellipse indicates the inshore area with

887 significant fluctuation.

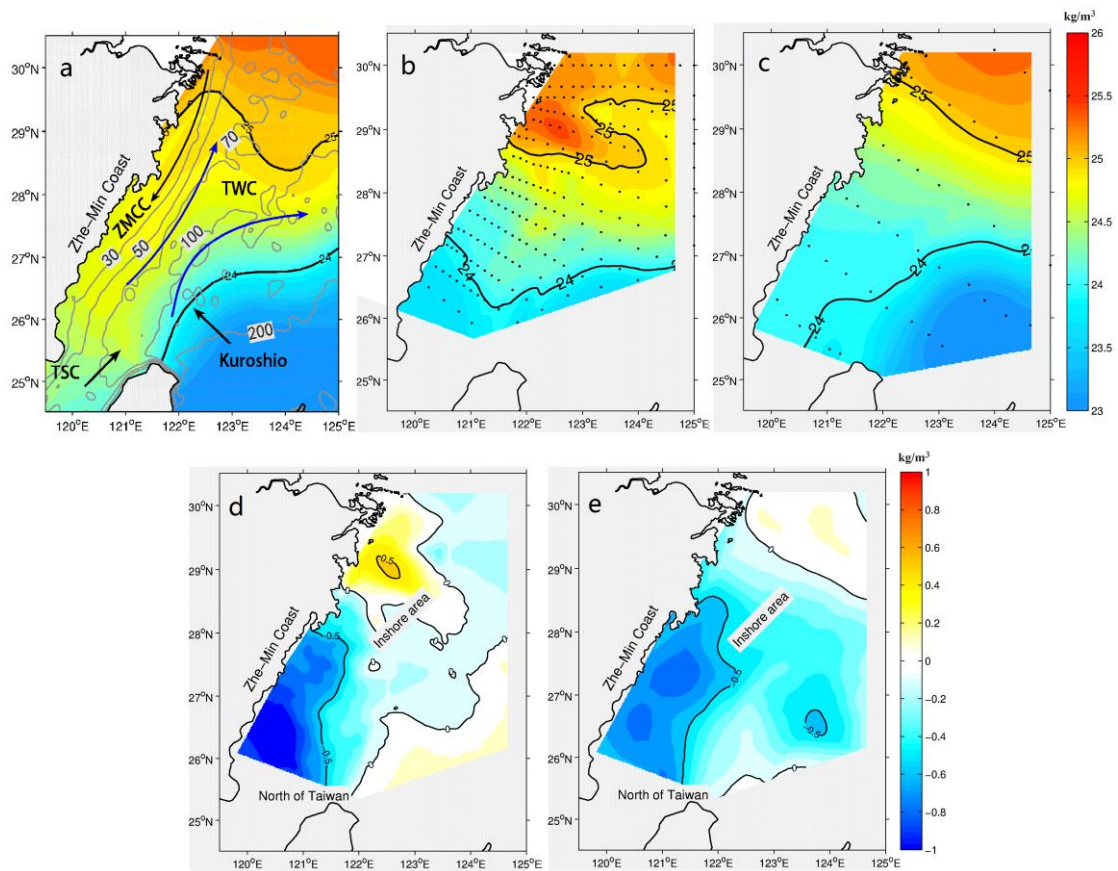
888

889 Table 1: Annual-mean volume transports ($S_v = 10^6 \text{ m}^3/\text{s}$) through various sections. The sections are
 890 shown in Figure 2 using blue dashed lines.

Section	Present model	Previous estimates
Taiwan Strait	1.22	1.2 (Isobe, 2008)
		1.8 (Wang et al., 2003)
		1.09 (Wu and Hsin, 2005)
		1.03 (Yang et al., 2011)
		1.72 (Guo et al., 2006)
		0.5 (Hung et al., 2003)
		1.10 (Liu et al., 2014b)
Tsushima Strait	2.85	2.65 (Isobe, 2008)
		3.03 (Guo et al., 2006)
		2.70 (Yang et al., 2011)
		2.52 (Liu et al., 2014b)
200m isobath	1.66	1.46 (Guo et al., 2006)
		0.87 (Liu et al., 2014a)
		3.0 (Teague et al., 2003)
		2.74 (Lee and Matsuno, 2007)
East Taiwan Channel	22.71	21.50 (Johns et al., 2001)
		23.00 (Teague et al., 2003)
		23.83 (Guo et al., 2006)
		28.4 (Hsin et al., 2013)
		21.37 (Yang et al., 2011)
		20.74 (Liu et al., 2014b)
Tokara Strait	23.20	23.4 (Feng et al., 2000)
		20.00 (Teague et al., 2003)
		20.66 (Yang et al., 2011)
		24.42 (Liu et al., 2014b)

891

892



894

895 Figure 1: Density (σ_t , kg/m^3) distributions at 50 m depth derived from the GDEM climatological data in

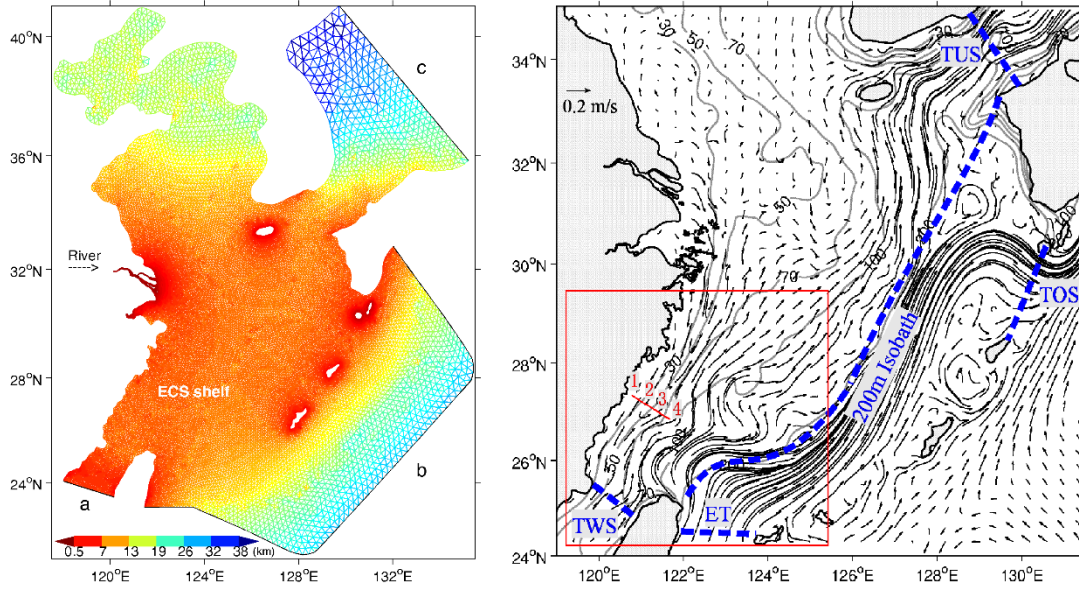
896 February (a), an ocean survey from Feb. 1–27, 2007 (b), and an ocean survey from Feb. 3–16, 2007 (c),

897 with the density anomalies between the GDEM data and the two surveys (d and e). The two blue arrows

898 indicate the two TWC branches in winter. The 30, 50, 70, 100 and 200 m isobaths are indicated with grey

899 lines in panel a.

900



901

902 Figure 2: The FVCOM model grid (Left) and the surface mean flow in the ECS in winter (Right). The

903 colors in the left panel show the grid length (km). The letters a, b, and c indicate the three open boundaries

904 at the Taiwan Strait, the northwest Pacific Ocean, and the Japan/East Sea, respectively. The blue dashed

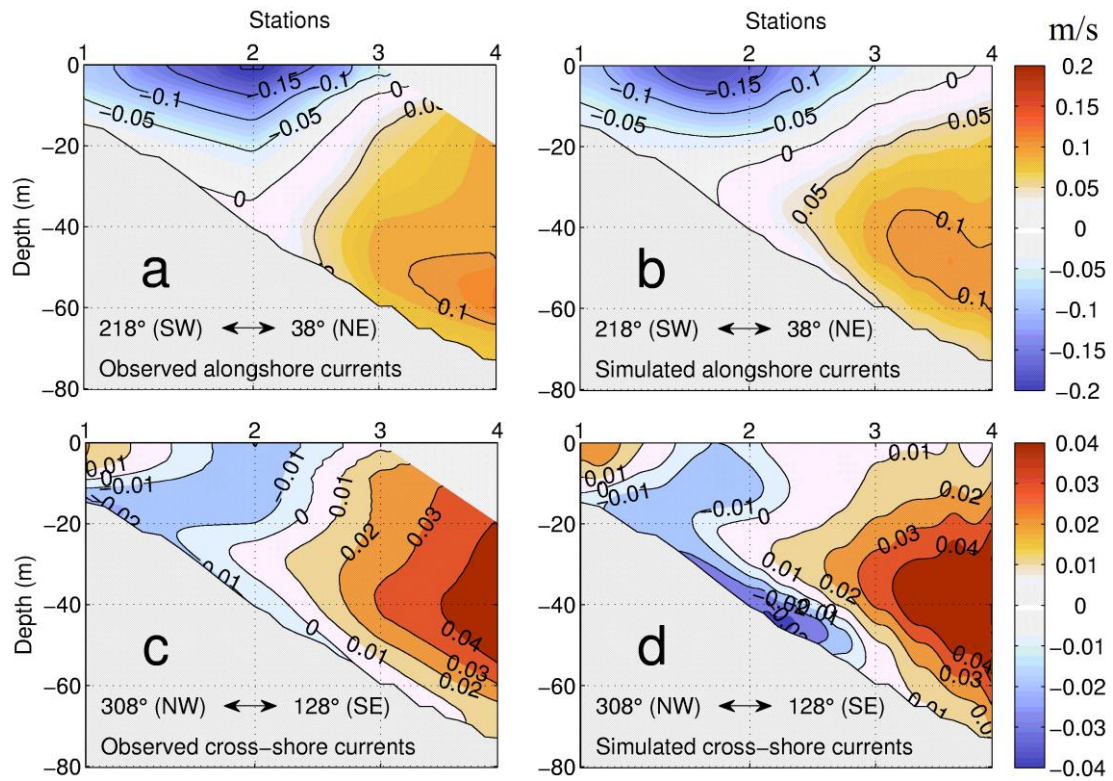
905 lines (right) show some important straits around shelf boundary, including the Taiwan Strait (TWS), the

906 East Taiwan Channel (ET), the Tsushima Strait (TUS), the Tokara Strait (TOS), and shelf break at the

907 200 m isobath. The red rectangle shows the study area of the wintertime TWC. The four red numbers off

908 the Zhe-Min coast shows the four mooring sites observed from Jan. 5 to Feb. 28, 2009.

909



910

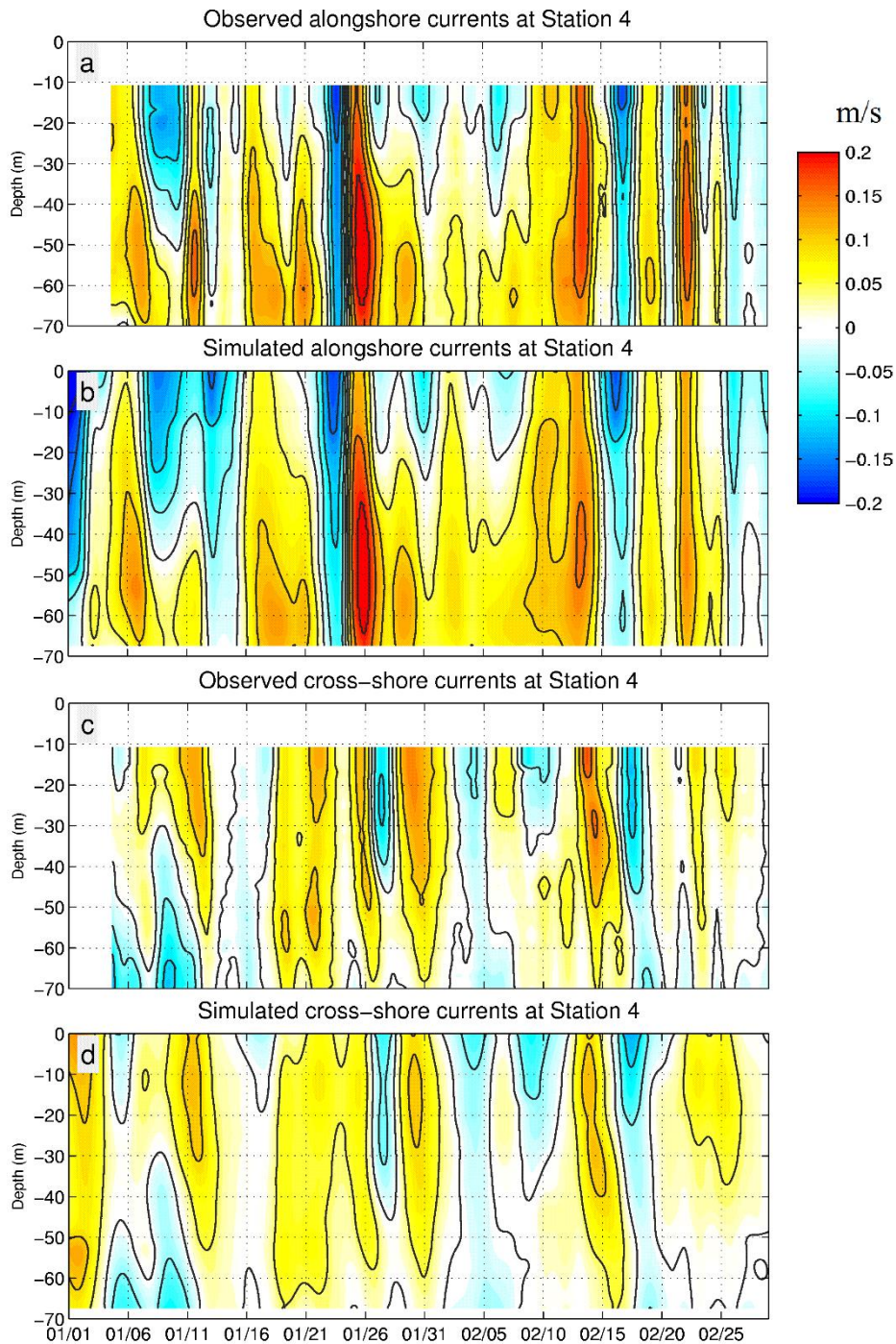
911 Figure 3: Validations of the wintertime TWC (warm color) along the section off the Zhe-Min coast (the

912 short line with four red numbers in Figure 2): (a) observed alongshore currents; (b) simulated alongshore

913 currents; (c) observed cross-shore currents; (d) simulated cross-shore currents. Note, an enlarged color

914 scale is used for the cross-shore component to have a clear view of its weak structure.

915



916

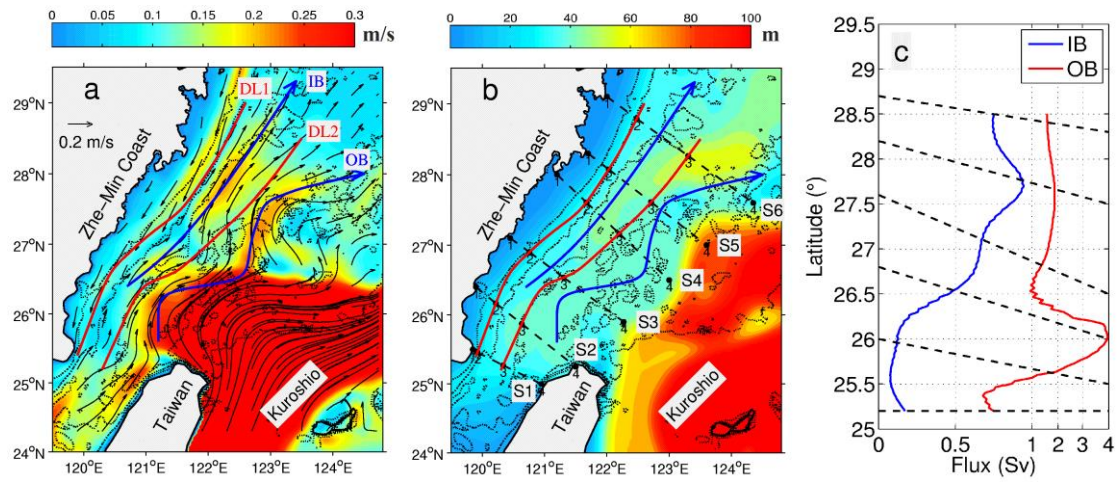
917 Figure 4: Variations of the inshore branch of TWC during January and February 2009: (a) observed

918 alongshore currents; (b) simulated alongshore currents; (c) observed cross-shore currents; (d) simulated

919 cross-shore currents. The observation data comes from Station 4 in Figure 1 and the simulated data has

920 the same position and period as the observation data.

921



922

923 Figure 5: a) Distribution of flow axes in the ECS in winter. The black arrows show the maximum velocity

924 (m/s) in the vertical profile (VMV) and the color shows the speed of the VMV. The two blue arrows with

925 label IB and OB represent the flow axes of the inshore branch and offshore branch, respectively. The red

926 line DL1 represents the dividing line between the coastal current and inshore branch, and the red line

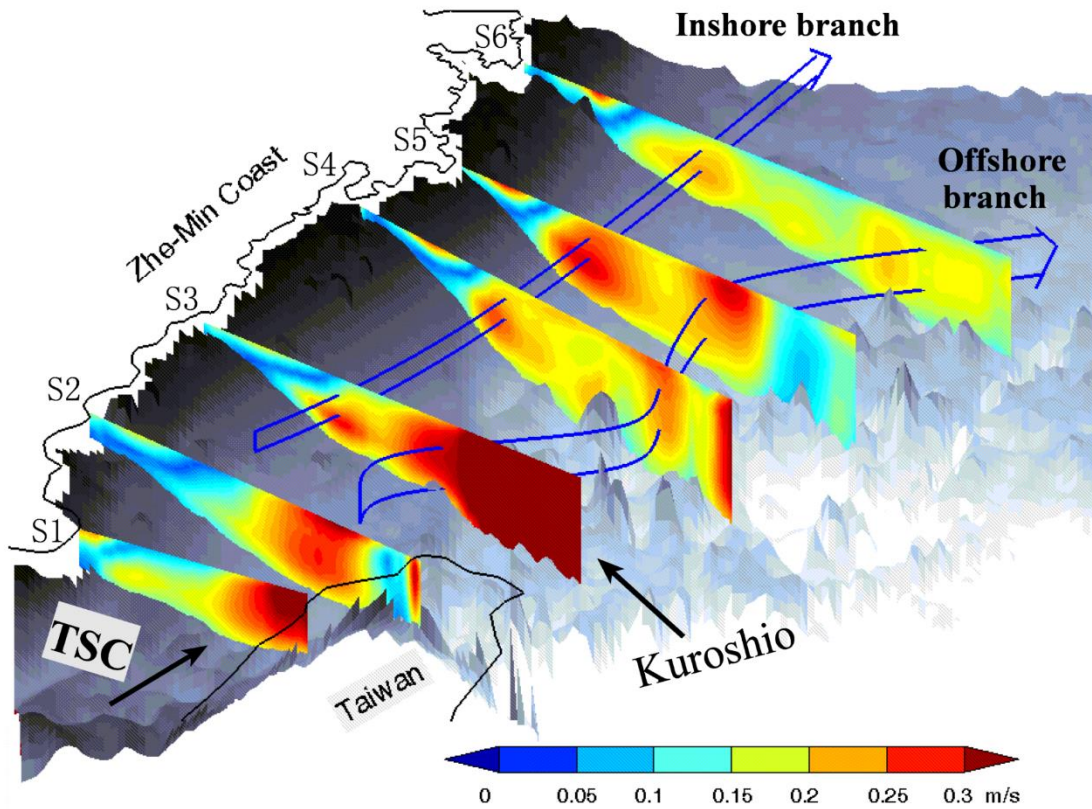
927 DL2 separates the two TWC branches. b) Depth (m) of flow axes in the ECS, shown by color. Sections

928 S1–S6 were selected to study the wintertime TWC. c) Flux of inshore branch (blue) and offshore branch

929 (red) at different latitudes. Dashed lines show the positions of Sections. S1–S6. Note, the scale is not

930 linear.

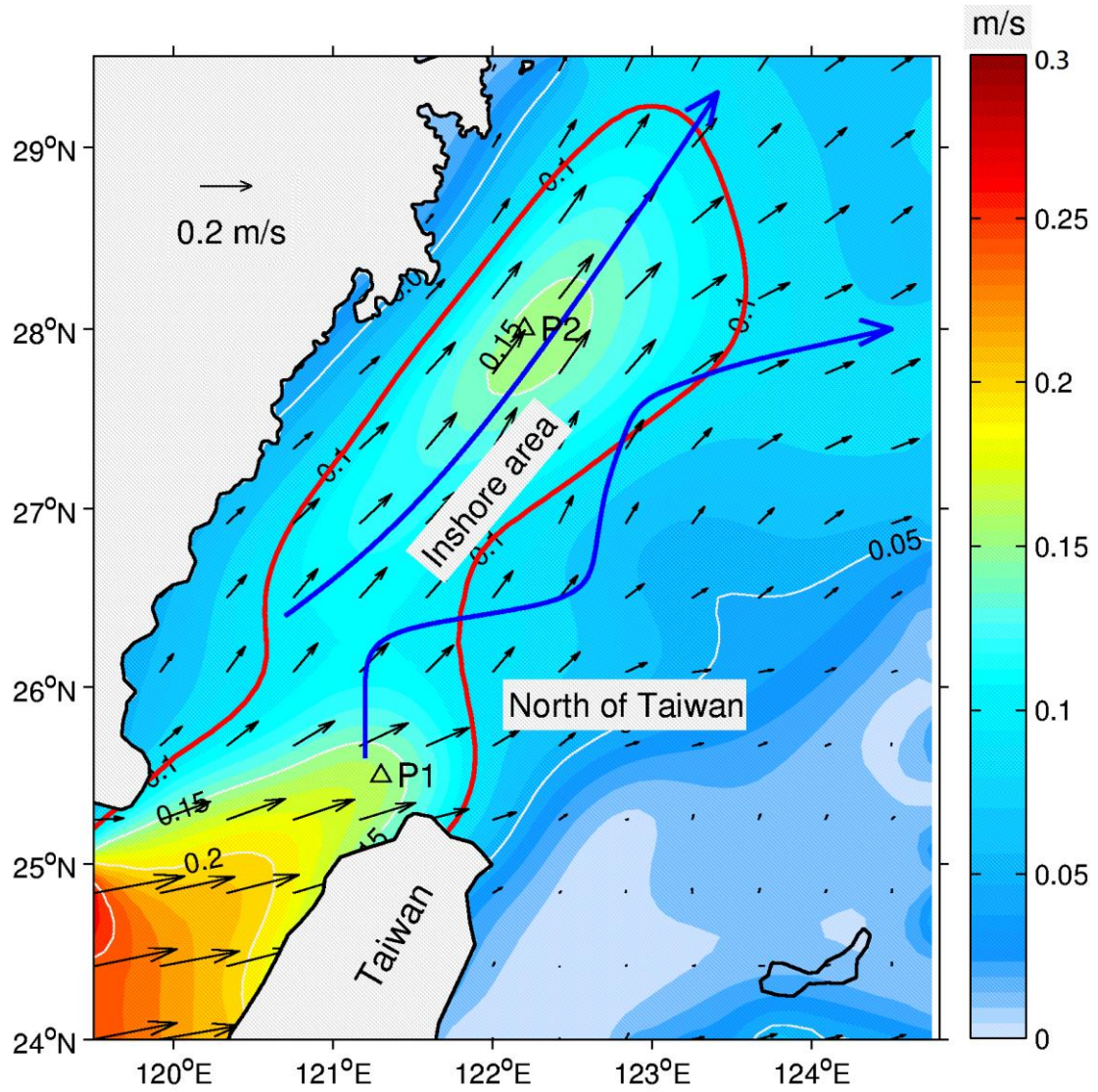
931



932

933 Figure 6: Distributions of current speed along the six sections S1–S6 in winter. The blue arrow on the
 934 left indicates the inshore branch according to the velocity cores from section S3 to S6. The blue arrow
 935 on the right indicates the offshore branch according to the velocity cores from section S2 to S6. TSC is
 936 the Taiwan Strait Current.

937



938

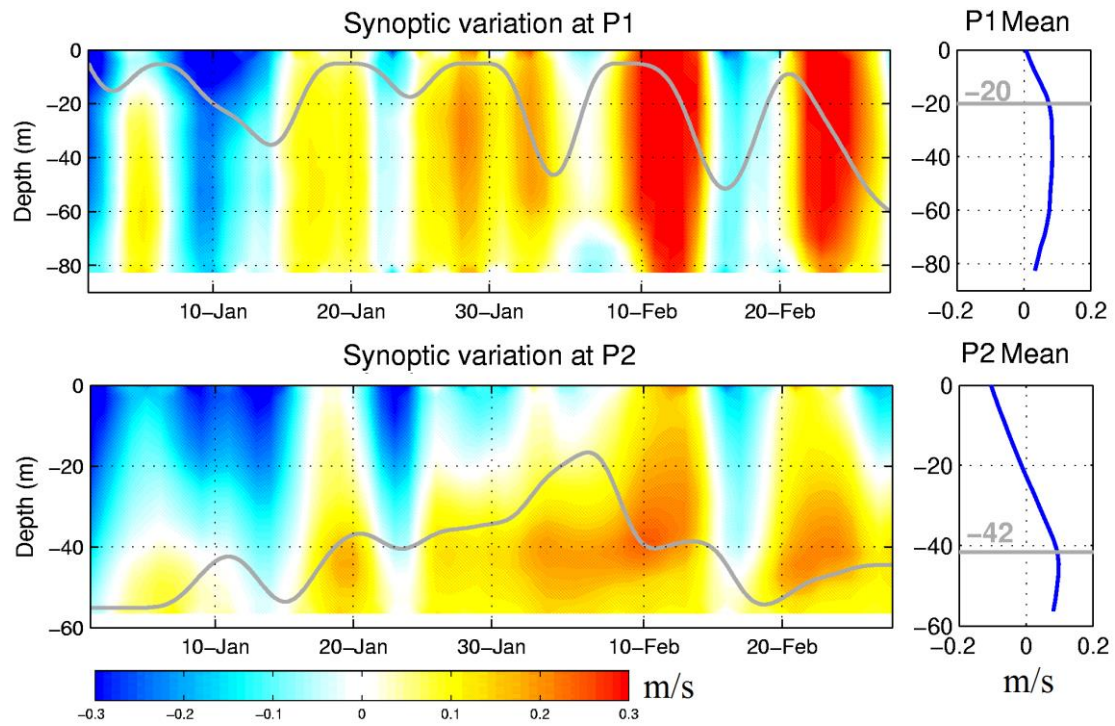
939 Figure 7: Current standard deviation (black arrows) in the layer of the VMV. The color shading shows

940 the magnitude of the current standard deviation. The two blue arrows indicate the two TWC branches.

941 The red curve indicate the area where the current standard deviation is larger than 0.1 m/s and their the

942 branches' representative points (P1 and P2) are selected for later analysis.

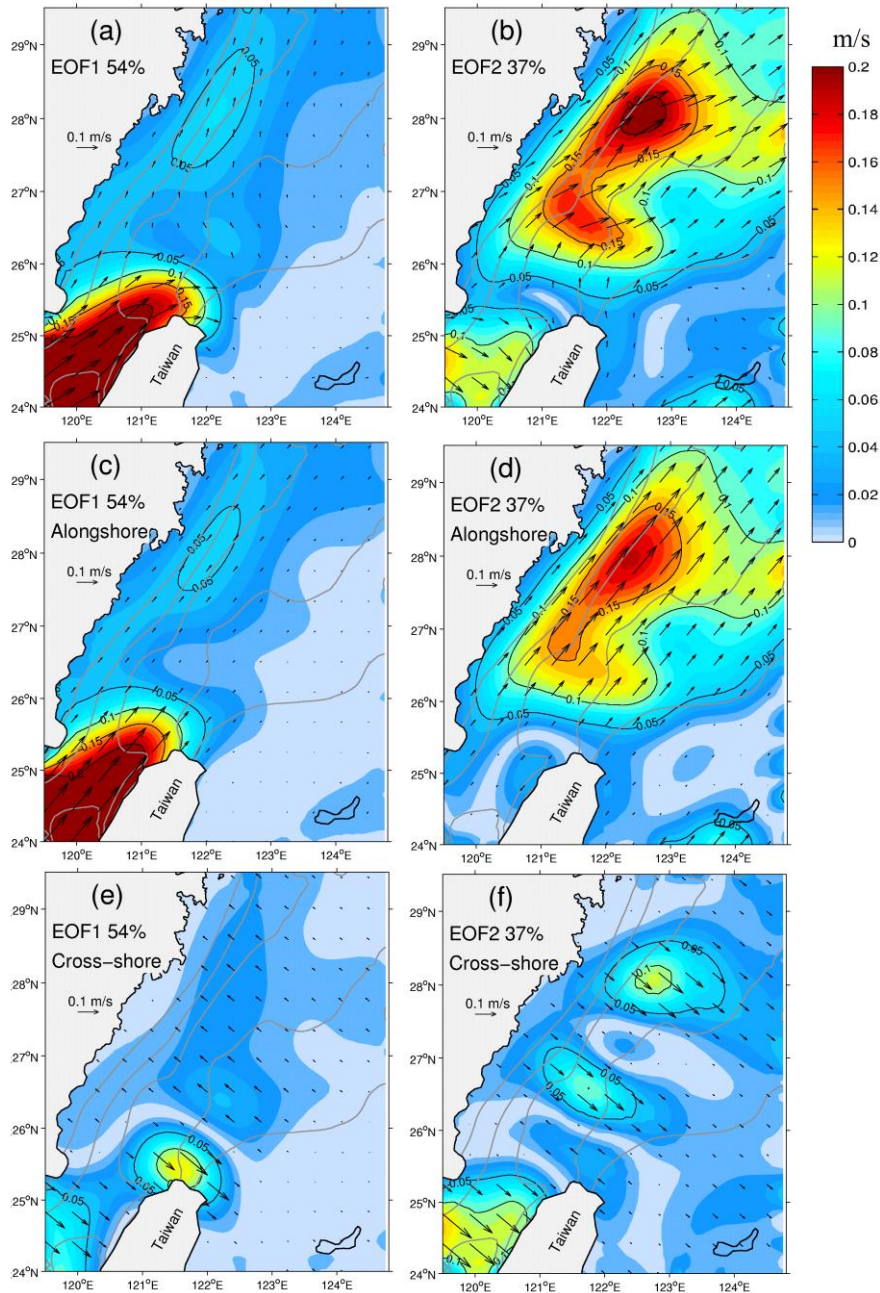
943



944

945 Figure 8: Variation of alongshore currents (m/s, shown by color scale) for the entire water column north
 946 of Taiwan (P1) and in the inshore area (P2) and their relation with upper mixed layer depth. The positive
 947 velocity (warm color) indicates the occurrence of the TWC. The gray solid lines show the depth of the
 948 upper mixed layer.

949



950

951 Figure 9: The spatial pattern of the first (EOF1; left) and second (EOF2; right) leading modes of the

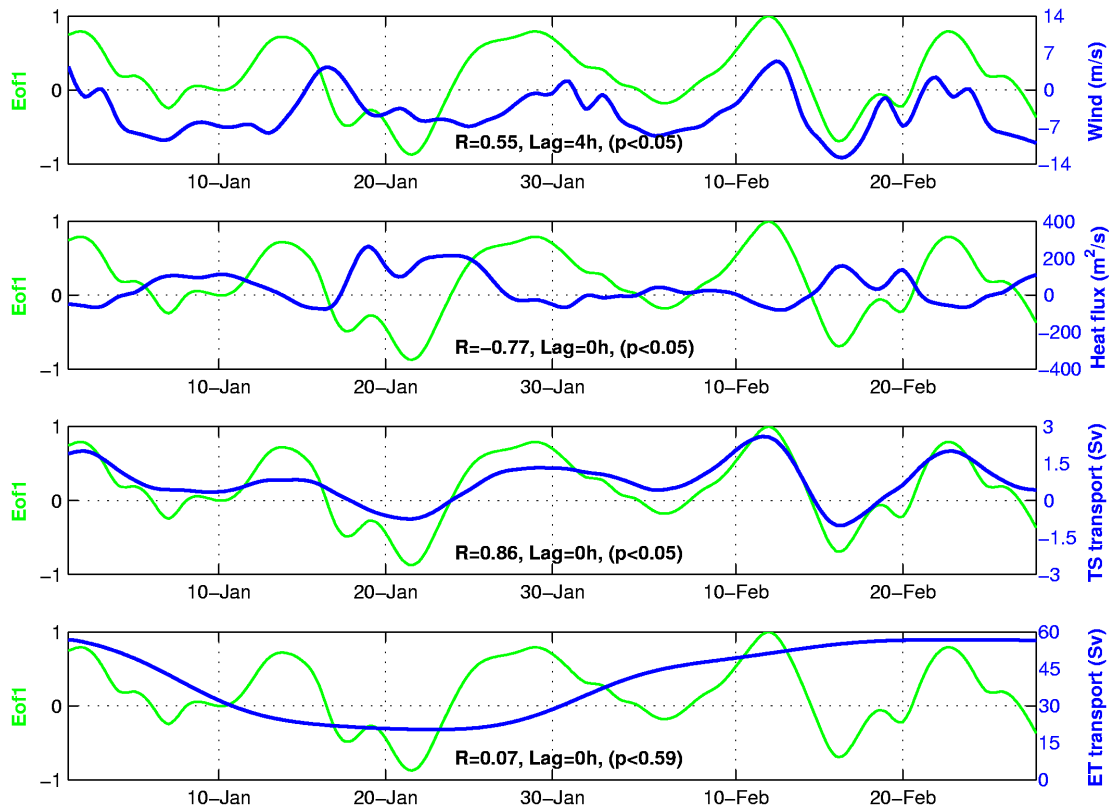
952 VMV in the ECS: (a) EOF1 currents, (b) EOF2 currents, (c) EOF1 alongshore component, (d) EOF2

953 alongshore component, (e) EOF1 cross-shore component, and (f) EOF2 cross-shore component (all

954 shown by black arrows with the color representing the magnitude). The 30, 50, 70, 100 and 200 m

955 isobaths are indicated with grey lines.

956



957

958 Figure 10: Temporal variation of EOF1, north-south component of wind speed, surface net heat flux, and

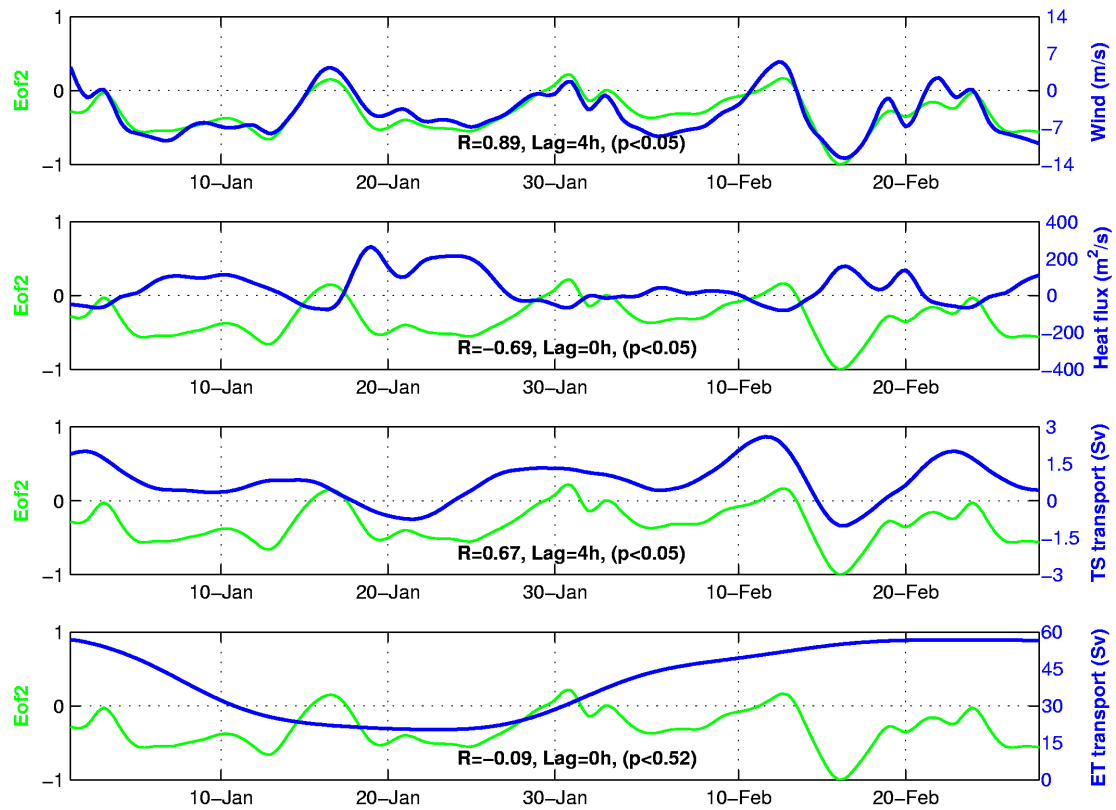
959 TSC flux along-across the TWS section, and Kuroshio flux alongacross the ET section. Their linear

960 correlation coefficients R and time-lags are also indicated in each panel. The p value is a declining

961 indicator which indicates the impact significance of the linear correlation coefficients R whereby R has

962 statistical significance and the confidence level is larger than 95% when the p value is less than 0.05.

963



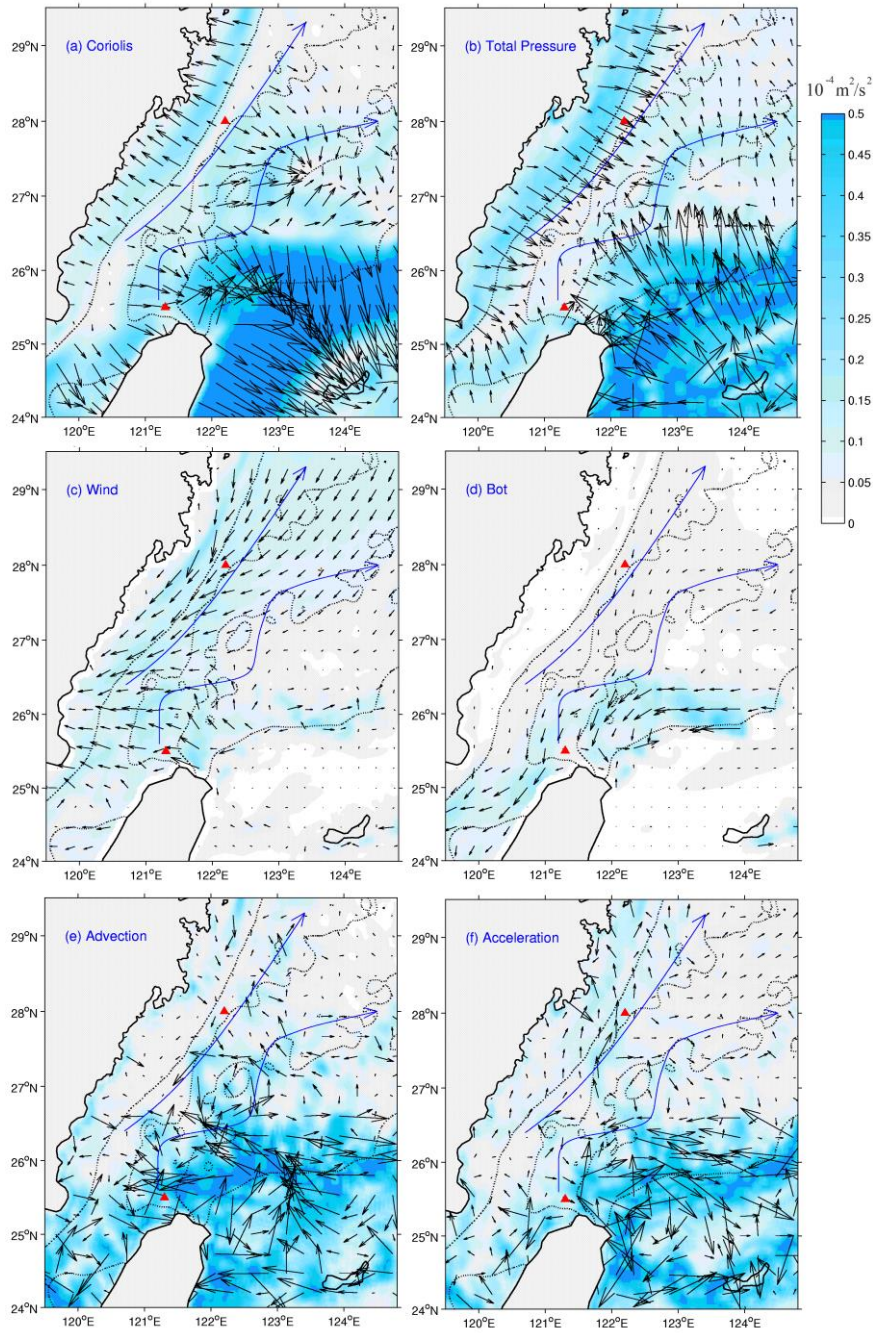
964

965 Figure 11: Temporal variation of EOF2, north-south component of wind speed, surface net heat flux, and

966 TSC flux along-across the TWS section, and Kuroshio flux along-across the ET section. Their linear

967 correlation coefficients and time-lags are also indicated in each panel.

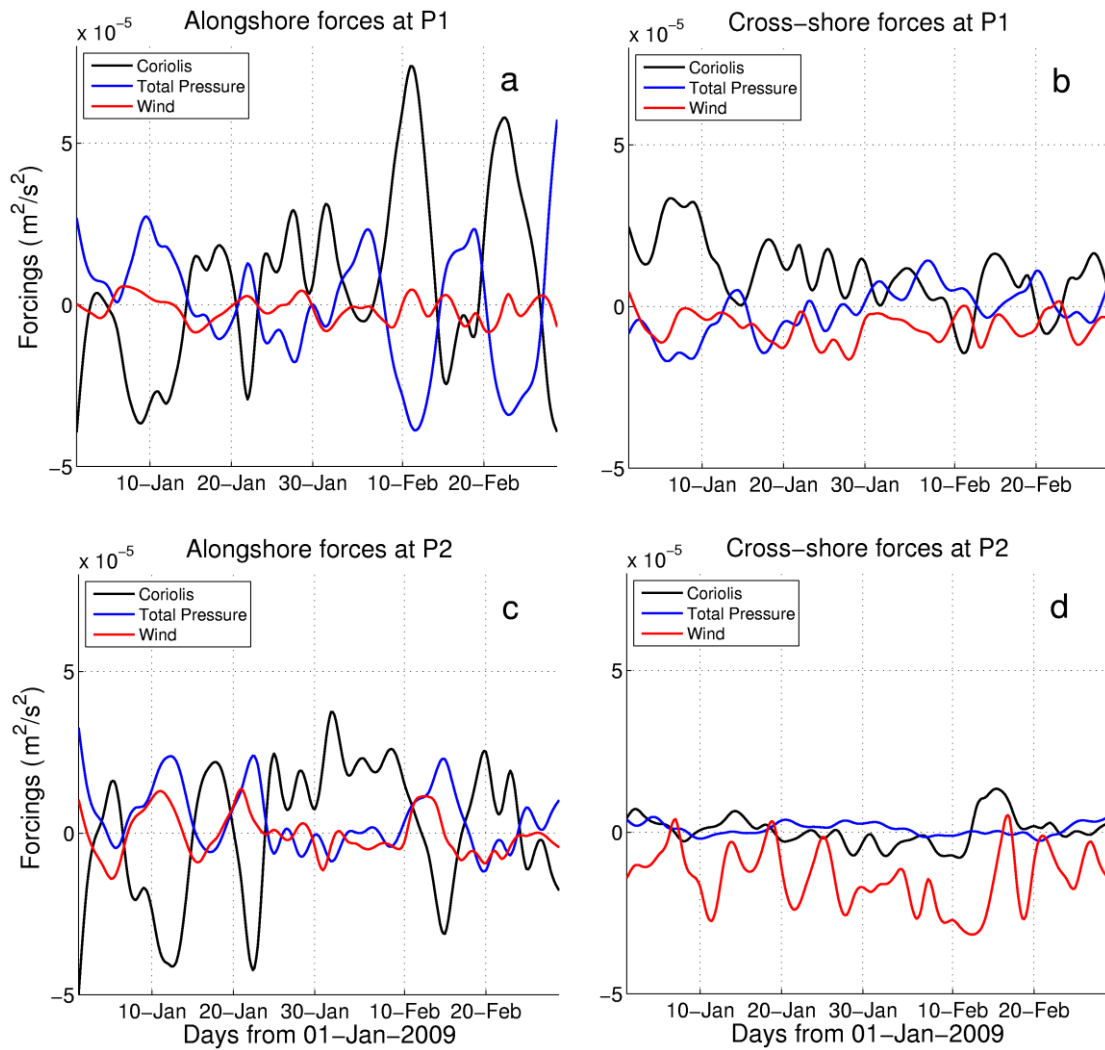
968



969

970 Figure 12: The effects of Coriolis force (a), total pressure (b), surface friction (c), bottom friction (d),
 971 advection (e), and local acceleration (f) for water column in winter according to Eq. (5) (shown by black
 972 arrows with the color representing the magnitude; units: $10^{-4} \text{ m}^2/\text{s}^2$). The two blue arrows indicate the
 973 two TWC branches. The two triangles indicate the two regions with significant fluctuation north of
 974 Taiwan (P1) and in the inshore area (P2).

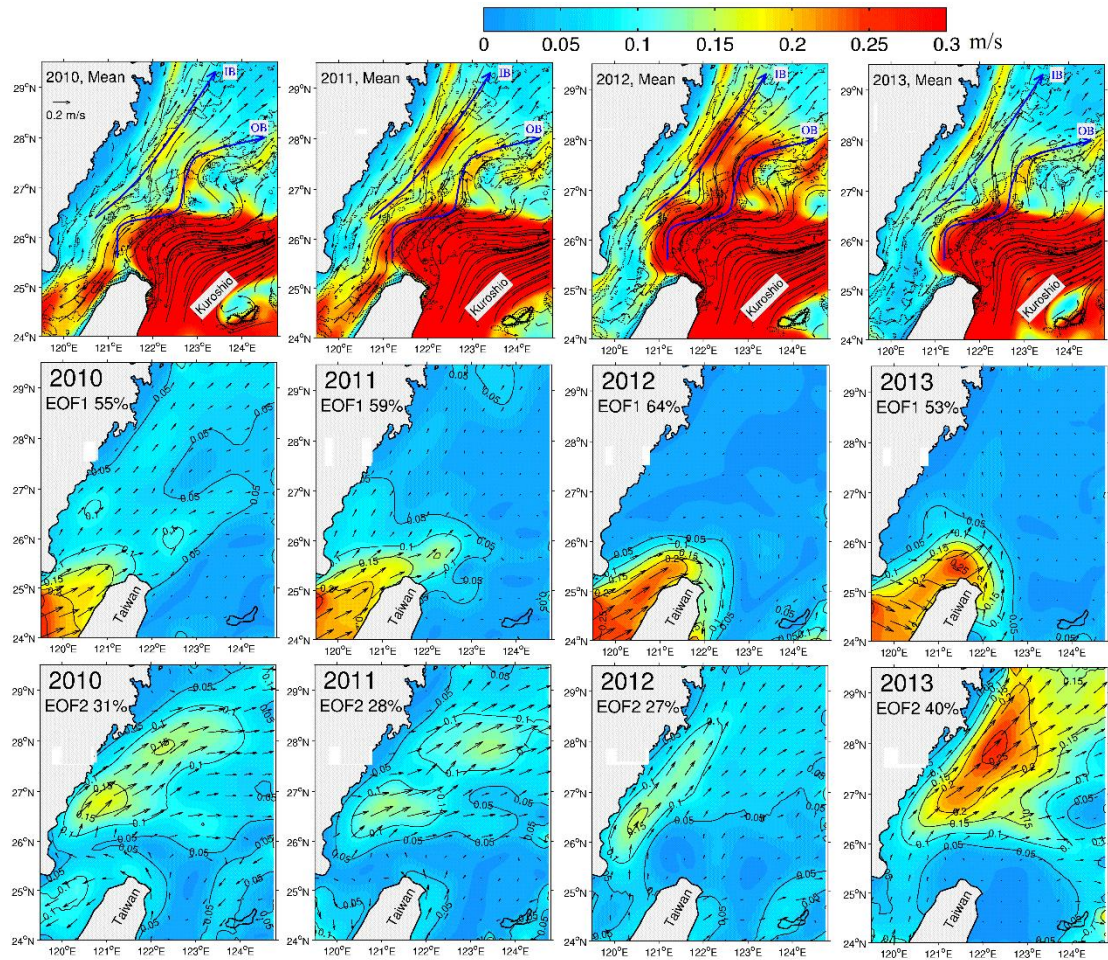
975



977

978 Figure 13: Variations in Coriolis force, total pressure, and wind in the alongshore direction at P1 (a), the
 979 cross-shore direction at P1 (b), the alongshore direction at P2 (c), and the cross-shore direction at P2 (d)
 980 according to Eq. (5).

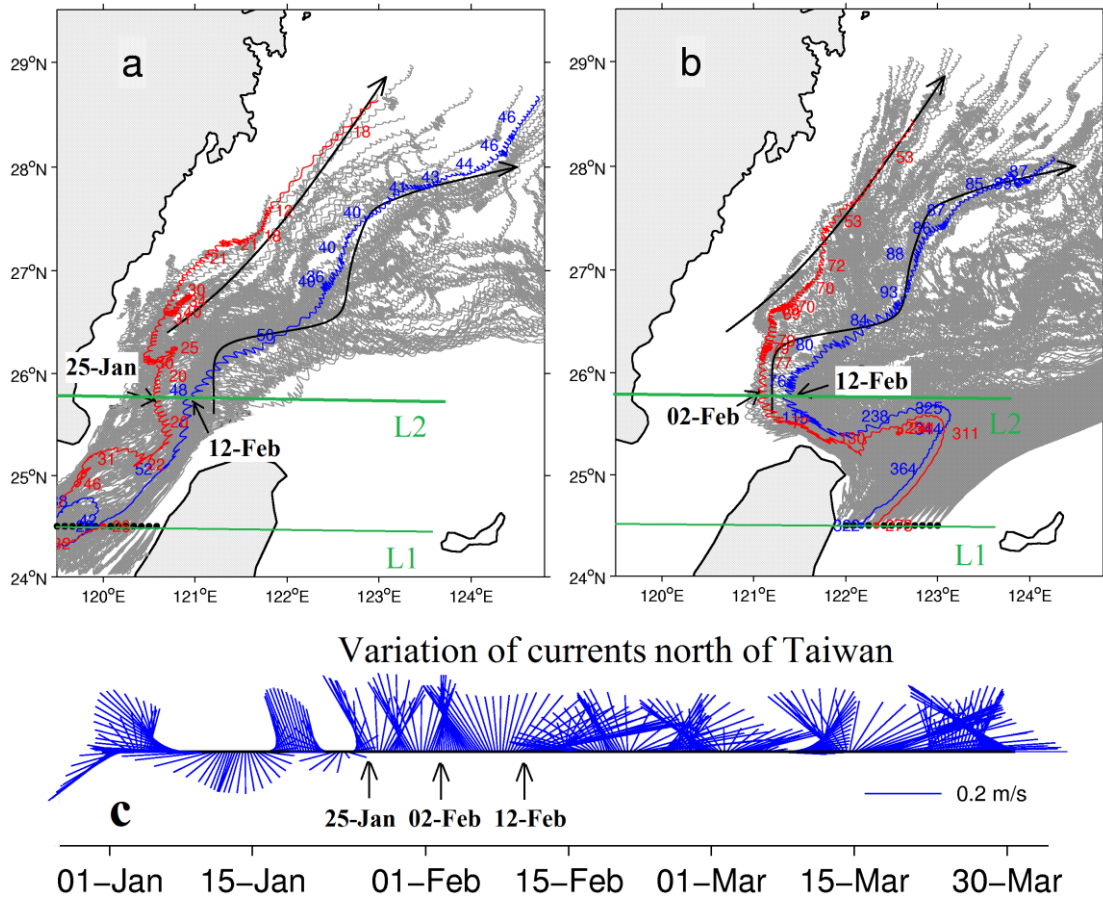
981



982

983 Figure 14: Mean currents (upper panels) and synoptic fluctuations (EOF1 in middle panels and EOF2 in
 984 bottom panels) in winters of 2010-2013. The black arrows in the upper panels show the velocity (m/s) in
 985 the layer of VMV and with the color representingshows the current speed. The two blue arrows with
 986 label IB and OB represent the flow axes of the inshore branch and offshore branch, respectively. The
 987 black arrows in the middle panels and bottom panels represent the EOF components (m/s) with their
 988 magnitude represented by color scales.

989



990

991 Figure 15: Traces of TSC water (a) and Kuroshio water (b) in winter, with the variation of surface currents

992 at the original location of P1 north of Taiwan (c). The green lines L1 and L2 indicate the starting latitude

993 of the tracers (24.5°N) and the latitude which is representative for synoptic fluctuations north of Taiwan

994 (25.8°N), respectively. The black dots represent the release locations of tracers originated from line L1.

995 The gray lines show the entire trajectories of the tracers. The red lines and blue lines are selected

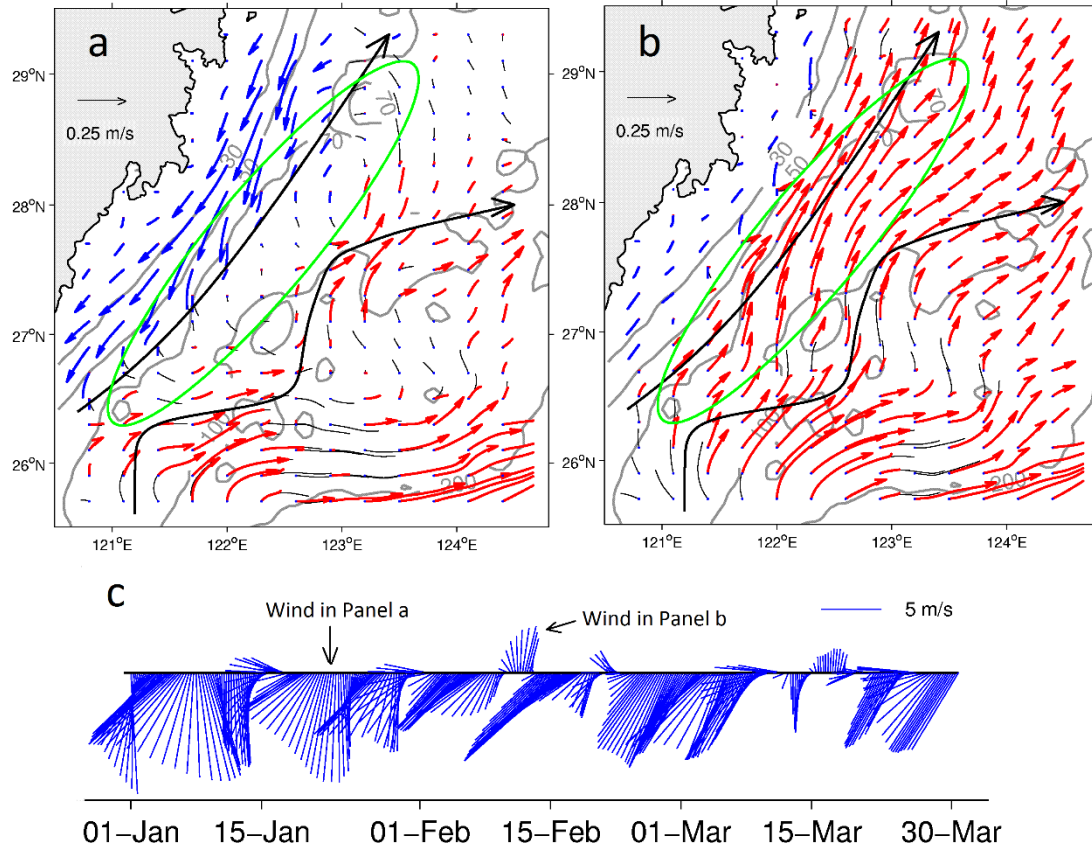
996 trajectories, which are close to the inshore branch and offshore branch, respectively. The dates show the

997 times that when selected tracers reached cross the origin latitude indicated by location P1 line L2; note

998 that the location of P1 is not fixed but varies with time. The numbers are the depths of the tracers, which

999 are labeled at an interval of six days. The two black arrows represent the two TWC branches.

1000



1001
 1002
 1003
 1004
 1005
 1006
 1007
 1008

Figure 16: The VMV under the northeasterly wind (a) and southwesterly wind (b). Panel (c) shows the variation of wind in winter. Blue vectors and red vectors show the southwestward coastal current and the northeastward TWC, respectively. Gray contours indicate the 30, 50, 70, and 100 m isobaths. The two black arrows represent the two TWC branches. The green ellipse indicates the inshore area with significant fluctuation.